Earth And Planetary Science Letters
May 2018, Volume 490 Pages 51-61
https://doi.org/10.1016/j.epsl.2018.03.006
https://archimer.ifremer.fr/doc/00497/60818/

Similar mid-depth Atlantic water mass provenance during the Last Glacial Maximum and Heinrich Stadial 1

Howe Jacob N. W. [1, 2], Huang Kuo-Fang [2, 3, *], Oppo Delia W. [2], Chiessi Cristiano M. [4], Mulitza Stefan [5], Blusztajn Jurek [2], Piotrowski Alexander M. [1]

[1] Univ Cambridge, Dept Earth Sci, Cambridge CB2 3EQ, England.
[2] Woods Hole Oceanog Inst, Dept Geol & Geophys, Woods Hole, MA 02543 USA.
[3] Acad Sinica, Inst Earth Sci, 128,Sec 2,Acad Rd, Taipei 11529, Taiwan.
[4] Univ Sao Paulo, Sch Arts Sci & Humanities, Av Arlindo Bettio 1000, BR-03828000 Sao Paulo, SP, Brazil.
[5] Univ Bremen, MARUM Ctr Marine Environm Sci, Leobener Str, D-28359 Bremen, Germany.

* Corresponding author : Kuo-Fang Huang, email address : kfhuang@earth.sinica.edu.tw

Abstract :

The delivery of freshwater to the North Atlantic during Heinrich Stadial 1 (HS1) is thought to have fundamentally altered the operation of Atlantic meridional overturning circulation (AMOC). Although benthic foraminiferal carbon isotope records from the mid-depth Atlantic show a pronounced excursion to lower values during HS1, whether these shifts correspond to changes in water mass proportions, advection, or shifts in the carbon cycle remains unclear. Here we present new deglacial records of authigenic neodymium isotopes - a water mass tracer that is independent of the carbon cycle-from two cores in the mid-depth South Atlantic. We find no change in neodymium isotopic composition, and thus water mass proportions, between the Last Glacial Maximum (LGM) and HS1, despite large decreases in carbon isotope values at the onset of HS1 in the same cores. We suggest that the excursions of carbon isotopes to lower values were likely caused by the accumulation of respired organic matter due to slow overturning circulation, rather than to increased southern-sourced water, as typically assumed. The finding that there was little change in water mass provenance in the mid-depth South Atlantic between the LGM and HS1, despite decreased overturning, suggests that the rate of production of mid-depth southern-sourced water mass decreased in concert with decreased production of northern-sourced intermediate water at the onset of HS1. Consequently, we propose that even drastic changes in the strength of AMOC need not cause a significant change in South Atlantic mid-depth water mass proportions.

Highlights

► We present two authigenic neodymium records from the mid-depth South Atlantic. ► These records show no change between the Last Glacial Maximum and Heinrich Stadial 1. ► Water mass provenance was similar at both sites during these time periods.

Keywords : Atlantic overturning, neodymium isotopes, Heinrich Stadial 1, Last Glacial Maximum

1. **Introduction**

The most recent glacial termination was apparently accompanied by changes in Atlantic meridional overturning circulation e.g. ref (Böhm et al., 2015; McManus et al., 2004) that are thought to be important in communicating changes in the climate between the Northern and Southern Hemispheres (Broecker, 1998). One key event in this transition was Heinrich Stadial 1 (HS1), a Northern Hemisphere cold period during which massive iceberg rafting into the North Atlantic occurred (Hemming, 2004). The freshwater from melting icebergs is believed to have reached the regions of deep water formation where it may have caused a weakening (Bond et al., 1992; Bradtmiller et al., 2014; Broecker, 1994; Gherardi et al., 2005; Oppo et al., 2015) or even a near-complete shut-down (McManus et al., 2004) of Atlantic overturning.

Benthic foraminiferal carbon isotope records from the intermediate (here, 1000-1500 m) and mid-depth (here, 1500-2500 m) Atlantic show pronounced excursions to low $\delta^{13}C$ values during HS1 (Lund et al., 2015; Oppo et al., 2015; Rickaby and Elderfield, 2005; Tessin and Lund, 2013; Thornalley et al., 2010; Zahn and Stüber, 2002). While it has long been recognized that changes in remineralization can impact $\delta^{13}C$ values (Curry and Lohmann, 1983), lower $\delta^{13}C$ values in the Atlantic are most commonly interpreted as a greater fraction of low-$\delta^{13}C$ southern-sourced water (SSW) (Boyle and Keigwin, 1987; Duplessy et al., 1988; Keigwin and Lehman, 1994; Sarnthein et al., 1994). However, several recent studies suggest the influence of remineralization on deglacial $\delta^{13}C$ may be greater than previously appreciated and that it may have contributed significantly to the observed HS1 $\delta^{13}C$ decrease (Lacerra et al., 2017; Oppo et al., 2015; Schmittner and Lund, 2015; Voigt et al., 2017). In addition to more SSW and greater remineralization, the LGM to HS1 $\delta^{13}C$ decrease has also been attributed to a decrease in the northern-sourced end-member $\delta^{13}C$ value (Lund et al., 2015; Waelbroeck et al., 2011). These explanations are not mutually exclusive and a recent study suggested that while a combination of these mechanisms could explain the LGM to HS1 $\delta^{13}C$ decrease in the mid-depth North and South Atlantic, their relative importance could not be determined on the basis of benthic $\delta^{13}C$ and $\delta^{18}O$ data alone (Oppo et al., 2015). This ambiguity limits our knowledge of how the water mass provenance within the Atlantic varied between the LGM and HS1. As a result, our fundamental understanding of how ocean circulation responds to perturbations such as the freshwater forcing thought to have occurred during HS1 still contains a significant element of uncertainty.

1.1 Neodymium isotopes

The isotopes of the radiogenic element neodymium (expressed as ε_{Nd}) act as quasi-conservative water mass tracer that is independent of the remineralisation of organic matter (Frank, 2002). In the modern Atlantic, ε_{Nd} ($^{143}Nd/^{144}Nd$ normalised to $^{143}Nd/^{144}Nd_{CHUR}$ = 0.512638, Hamilton et al., 1983; Jacobsen and Wasserburg, 1980) in parts per ten thousand) distinguishes upper North Atlantic Deep Water (NADW) (-13.2) (Lambelet et al., 2016) in the subtropical North Atlantic from both Antarctic Intermediate Water (AAIW) (-8.3) and Antarctic Bottom Water (AABW) (-8.5) (Stichel et al., 2012). In addition, the conservative behavoir of seawater Nd isotopes has been suggested for intermediate/deep depths of the Atlantic Ocean (i.e. around 2500 m and below) (Goldstein and Hemming, 2003; Lambelet et al., 2016). As a result, neodymium isotopes are the ideal candidate to investigate whether the low-$\delta^{13}C$ values observed in the mid-depth Atlantic during HS1 were the result of changes in water mass provenance. Although numerous deglacial records of authigenic neodymium isotopes from throughout the Atlantic do exist (Gutjahr et al., 2008; Huang et al., 2014; Lippold et al., 2016; Piotrowski et al., 2004; Roberts et al., 2010; Skinner et al., 2013; Wei et al., 2016), the mid-depth Atlantic - a key region for understanding how Atlantic overturning varied between the LGM and HS1 - remains underinvestigated. In this paper we present two deglacial foraminiferal ε_{Nd} records from the mid-depth South Atlantic. These ε_{Nd} records display little change between the LGM and HS1. Although uncertainty remains in the neodymium composition of water mass end-members during these time periods, we propose that the simplest explanation for this lack of change in ε_{Nd} values is that the provenance of the water masses in the mid-depth Atlantic was similar during the LGM and HS1. This interpretation suggests that the low $\delta^{13}C$ values observed in the mid-depth South Atlantic during HS1 were caused by other mechanisms, most likely the greater accumulation of organic matter in slower circulating water (Lacerra et al., 2017; Voigt et al., 2017).

2. Materials and Methods

2.1 Core sites

KNR159-5-33GGC (27.6°S, 46.2°W, 2082 m; 33GGC hereafter) and GL1090 (24.9°S, 42.5°W, 2225 m) were cored on the southern Brazil margin in the South Atlantic (Fig. 1). The age model of 33GGC is based upon planktic foraminiferal radiocarbon dates (Tessin and Lund, 2013) and yields a sedimentation rate of 27 cm/kyr in the deglacial section and 2 cm/kyr in the Holocene (Tessin and Lund, 2013). The age model for GL1090 was constructed using planktic foraminiferal radiocarbon dates (Santos et al., 2017) converted to calendar ages using the Marine13 calibration (Reimer et al., 2013); this is the same method as applied in the original study (Santos et al., 2017). The average sedimentation rate in the glacial and HS1 section of the core is 8 cm/kyr, and from the Bølling-Allerød onwards is 3.5 cm/kyr. Although some parameters used to produce the age models of the two cores are slightly different (Santos et al., 2017; Tessin and Lund, 2013) these slight variations are less than the resolution of the sampling of each core. The age model of core SU90-03 that is used for comparison in this work was constructed using radiocarbon ages obtained nearly 20 years ago (Chapman and Shackleton, 1998) and as such the effect of more recent reservoir age estimates should be considered. Although there are many radiocarbon measurements available on core SU90-03 the species measured varies greatly and there are numerous age reversals (Chapman and Shackleton, 1998; Chapman et al., 2000). Therefore we used available counts of small grains of ice rafted detritus (Chapman and Shackleton, 1998) to constrain the time period of HS1 in the age model of SU90-03, the most important time period for our study. A full description of the revised age model together with a comparison between the revised age model and the original one from Chapman and Shackleton (1998) are given in the supplementary file.

2.2 Neodymium measurements

Planktic foraminifera were picked from the coarse fraction (>63, >42, >35 or >25 μm) of both cores and then processed following the method described in ref. (Roberts et al., 2010). The detrital fractions of cores 33GGC and GL1090 were prepared for analysis following ref. (Bayon et al., 2002). Rare earth elements from both foraminiferal and detrital samples were separated using Eichrom TRU Resin, and then neodymium was separated from the other rare earth elements using Eichrom LN resin loaded on volumetrically calibrated Teflon columns. Samples from GL1090 were analysed for isotopic composition on a Neptune Plus multi collector inductively coupled mass spectrometer (MC-ICP-MS) in the Department of Earth Sciences at the University of Cambridge. Samples from 33GGC were analysed on a Neptune MC-ICP-MS at Woods Hole Oceanographic Institute (Huang et al., 2012). Isotopic ratios were corrected to a $^{144}Nd/^{146}Nd$ of 0.7219. Samples were bracketed with the reference standard JNdi-1 that was corrected to the accepted value of $^{143}Nd/^{144}Nd$ = 0.512115 (Tanaka et al., 2000). Error bars correspond to 2σ of external reproducibility of the bracketing standards except for when the internal error was larger than the external error, in which case the error quoted is the combined error. The average ε_{Nd} external reproducibility was ±0.15 for the Neptune Plus and ±0.40 for the Neptune. All results are listed with errors in Tables S2, S3 and S4.

2.3 LGM and HS1 compilation sections

Data measured in this work were collated with published data to construct meridional sections of the Atlantic during the LGM and HS1. For the LGM section, the data set from Howe et al (2016) was updated with data from this work and Lippold et al (2016) (Table S6) using the time window 23-19 ka. Data for the HS1 section were taken from authigenic ε_{Nd} records from sediment cores as well as coral measurements within the time period 17.5-15 ka (references in Table S5). Coral results from the New England seamounts dated from HS1 (van de Flierdt et al., 2006; Wilson et al., 2014) were binned into 100 m depth windows and were averaged for each depth. Core locations are plotted in Fig. S2. Leachate records from sites where the core top values do not match nearby seawater were excluded from both sections. The minimum number of data points required for a site to be included within each time period was one. For the 22 cores were data are available the difference between the average values for each time period was calculated along with an estimate of the error associated with the difference (Table S7).

3. **Results and discussion**

3.1 Veracity of neodymium isotopes

The core top foraminiferal ε_{Nd} value of 33GGC (-10.4±0.4) agrees well with the interpolated values from nearby seawater (Fig. 2, Jeandel, 1993) consistent with an authigenic foraminiferal signal derived from seawater. The core top foraminiferal ε_{Nd} value of GL1090 (-13.0±0.1) is less radiogenic than that of 33GGC and of the least radiogenic ε_{Nd} value observed from nearby seawater (-12.3±0.4; Jeandel, 1993) . There are a number of possible explanations for the 2.6 ε unit difference in the core top values of these two close cores, as well as for the core top value of GL1090 being less radiogenic than the nearest seawater profile.

First, although the sites of cores 33GGC and GL1090 are separated by only ~150 m water depth, they are located at 27.6°S and 24.9°S, respectively. This region has a strong water mass mixing gradient with a greater proportion of northern-sourced water (NSW) at more northerly latitudes, as can be seen from the salinity contours in the region (Fig. 1). Furthermore the nearest ε_{Nd} seawater profile (SAVE 302, 33.6°S, 41.6°W; Jeandel, 1993) exhibits a gradient of -0.30 ε units per 100 m of increasing depth from ~1600 m to ~2800 m (Fig. 2). A strong spatial gradient is also seen in seawater neodymium isotopes at similar depths in the eastern South Atlantic. There, water at 25°S and 2024 m water depth has an ε_{Nd} value of -12.5 (Station 69/26, Rickli et al., 2009) whilst water from 30°S and 1835 and 2443 m water depth have values of -11.1 and -11.0 respectively (SAVE 217, Jeandel, 1993). This represents a gradient of 1.5 ε units within 5 degrees of latitude and just 200 m water depth difference. These seawater data indicate that cores 33GGC and GL1090 are located in a region of both strong horizontal (Fig. 1) and vertical (Fig. 2) epsilon neodymium gradients, as would be expected near a water mass boundary, thereby explaining how cores so close to one another can record very different neodymium isotope signals.

Notwithstanding the water mass boundary effect, if the same 1.5 ε unit shift observed in seawater from similar depths in the southeast Atlantic were applied to the core top of 33GGC (-10.4±0.4) the predicted core top value of GL1090 would be -11.9±0.4, whereas the actual value is -13.0±0.1. Although the exact water mass distribution would be expected to differ slightly between the eastern and the western South Atlantic the comparison is valuable as the water mass boundaries should be similar. Gridding and interpolating the available seawater data from the Atlantic further supports this finding that the core top of GL1090 is approximately one ε unit less radiogenic than modern seawater (Fig. S3).

Second, the 6.8 ka age of the core top sample from GL1090 may in part explain the discrepancy between the foraminiferal ε_{Nd} value and that interpolated from seawater measurements (Figs. 2, S2). The non-modern age of the GL1090 core top, which is common for cores around this depth in this region (Tessin and Lund, 2013), means that the core top foraminiferal ε_{Nd} value is not necessarily directly comparable to modern seawater. Most mid-depth and deep Atlantic sites display trends to more radiogenic values in the mid- to late Holocene (e.g. Howe et al., 2016b; Lang et al., 2016; Lippold et al., 2016; Roberts et al., 2010; Skinner et al., 2013) thus the core top value of GL1090 may reflect the less radiogenic neodymium composition of Atlantic seawater during the mid-Holocene.

Third, whilst this mid-Holocene age of the GL1090 core top likely to explains part of the core top-seawater foraminiferal ε_{Nd} offset, the possibility of some diagenetic overprinting on the authigenic signal with detrital-derived neodymium cannot be ignored. The core top detrital value of GL1090 - which is consistent with published data from the region (de Mahiques et al., 2008) - is sufficiently unradiogenic (-13.8±0.3; Fig. 3) that diagenetic overprinting of the authigenic foraminiferal signal with detrital neodymium could cause slightly less radiogenic values than seawater to be preserved. Given the aforementioned impact of the age of the core top, we estimate that of the 1 ε unit discrepancy between the core top and seawater ε_{Nd} values, the offset due to detrital overprinting is on the order of 0.5 ε units.

The potential impact of this detrital overprinting down-core must also be considered. The deglacial detrital record ε_{Nd} of GL1090 shifts from glacial values around -11.5 to Holocene values around -14, whilst the foraminiferal record shifts from a glacial average of -10.9 to a Holocene average of -13.4 (Fig. 3b). Both records also exhibit a similar pattern of change across the deglaciation. The trend of both detrital and foraminiferal neodymium isotopes shifting to less radiogenic values across the deglaciation seen at GL1090 is, however, common amongst cores from the Atlantic (Howe et al., 2016b), thus the strong correlation between the two records does not imply that the entire down-core record is being controlled by local detrital overprint. Indeed, the average glacial foraminiferal value of GL1090 is -10.9 (Fig. 3b), whereas a study that compiled glacial values and interpolated an LGM section of the Atlantic Ocean predicted a value of between -10 and -10.5 for that site (Fig. 3, of Howe et al., 2016). This comparison of observed and expected glacial values would therefore support the existence of only a small detrital overprint, ~0.5 ε units, during the LGM as we have proposed for the core top value.

Furthermore, the deglacial foraminiferal U/Mn record of GL1090 (see methods on the supplementary material) only shows elevated values during the Holocene and the transition from the LGM to HS1 (Fig. S4). U/Mn can be used as a proxy to infer past changes in the oxygenation state of pore waters (Boiteau et al., 2012). The elevated U/Mn values during early HS1 imply less well oxygenated pore waters, and may reflect changes such as slower circulating water (Böhm et al., 2015; McManus et al., 2004) or greater delivery of organic matter to the sediments (Poggemann et al., 2017). Meanwhile the elevated U/Mn values in the Holocene likely reflect the considerable decrease in sedimentation rate of site GL1090 as sea level increased across the deglaciation and trapped a large fraction of the terrigenous sediments on the continental shelf (Lantzsch et al., 2014). The U/Mn record does not, however, suggest there is any relation between the oxygenation state of the pore waters of GL1090 and the foraminiferal ε_{Nd} values as, for example, the ε_{Nd} values are very similar during the LGM and HS1 (Fig. 3b) when the oxygenation state of the pore waters appears to have been dramatically different (Fig. S4). Al/Ca ratios measured on uncleaned foraminifera samples of GL1090 were below 100 μmol/mol in 16 of 19 samples. The three samples with values above 100 μmol/mol may indicate clay contamination of the samples, but shows no significant relation between the extracted ε_{Nd} and Al/Ca values. Furthermore, the rare earth element profiles of GL1090 (see methods on the supplementary material) exhibit MREE enrichment patterns typical of foraminifera (Fig. S6), not strongly detrital-type profiles (Neto and Figueiredo, 1995). PAAS-normalized HREE/LREE (Tm+Yb+Lu/La+Pr+Nd) vs. MREE/MREE* (Gd+Tb+Dy/average of HREE+LREE) of the uncleaned planktonic foraminifera samples (Fig. S5) fall within the range defined by HH-extractions, fish teeth, nodules, pore waters, as well as cleaned and uncleaned foraminifera of previous studies (Martine et al., 2004 and references therein), suggesting that detrital contributions do not significantly affect the REE contents of the Fe-Mn coatings extracted from uncleaned foraminifera. Therefore, we conclude that although there is evidence for a detrital overprint of the foraminiferal signal from GL1090 it is on the order of 0.5 ε units, and the detrital neodymium composition is not controlling the down-core foraminiferal record. The interpretations below for the authigenic ε_{Nd} record of GL1090 are valid under the assumption that there was no significant detrital overprint on the down-core ε_{Nd} record.

The foraminiferal and detrital ε_{Nd} records of 33GGC show both different timings and magnitudes (Fig. 3a). These differences imply that the detrital composition does not control the foraminiferal record, and there is no evidence to suggest that the foraminiferal record of 33GGC is being overprinted by detrital material given the excellent agreement of the core top value with nearby seawater (Fig. 2) (Jeandel, 1993).

3.2 Deglacial evolution of South Atlantic water mass provenance

The ε_{Nd} record of GL1090 consistently displays less radiogenic values than 33GGC over the past 25 kyr (Fig. 4), suggesting that the deeper site was always bathed by a greater proportion of NSW. This offset is likely because site GL1090 is located both ~ 150 m deeper but also ~ 300 km further north than 33GGC, placing it in the tongue of upper NADW in the modern Atlantic (Fig. 1). 33GGC on the other hand, is situated in the transition zone between this upper NADW and Upper Circumpolar Deep Water (UCDW)/AAIW in the modern ocean (Fig. 1). Our results, however, suggest that these water mass boundaries were not always in these locations over the past 25 kyr.

During the LGM and the early deglaciation 33GGC exhibits ε_{Nd} values between -9 and -10, within error of values at two intermediate depth (~1000-1250 m) nearby sites on the southern Brazil margin (GeoB2104-3 and KNR159-5-36GGC; Fig. 4, Howe et al., 2016a) suggesting that 33GGC was bathed almost exclusively by southern-sourced water at those times. During the late deglaciation (after ~ 14 ka) the 33GGC record begins to shift to less radiogenic values (peaking near -11 in the mid-Holocene), thereby diverging from the intermediate depth sites. This shift to less radiogenic values suggests a greater proportion of NSW at 33GGC and could represent the tongue of upper NADW extending further southwards across the deglaciation.

GL1090 shows less radiogenic values during the Holocene (around -13 to -14) than during the LGM and HS1 (mostly -10 to -11) (Fig. 4). The LGM and HS1 values reflect a mixture of NSW and SSW at those times (Howe et al., 2016), so the trend towards less radiogenic values after HS1 is consistent with a decreasing proportion of SSW (Roberts et al., 2010). By the Younger

Dryas ε_{Nd} values are typical of modern upper NADW (Fig. 4; Lambelet et al., 2016). The ε_{Nd} values of GL1090 and SU90-03, from similar depths in the South and North Atlantic respectively, are remarkably similar for most of the past 25 kyr, except during HS1 when North Atlantic values are slightly less radiogenic (Fig. 5). This similarity suggests the provenance of the water masses bathing SU90-03 in the North Atlantic was almost the same as that bathing GL1090 throughout the past 25 kyr.

GL1090 exhibits slightly less radiogenic values than SU90-03 during the early Holocene, possibly reflecting slightly greater proportion of unradiogenic Labrador Sea Water (Lambelet et al., 2016) in the slightly shallower core or alternatively the slight diagenetic overprint of unradiogenic sediments on the authigenic signal of GL1090 as discussed earlier. It is also worth noting that less radiogenic values than those seen at SU90-03 have been observed at a number of other sites in the North Atlantic (Lang et al., 2016; Lippold et al., 2016; Roberts et al., 2010). In contrast to the similarity to SU90-03, GL1090 shows less radiogenic values than a site from the deep (i.e., 3770 m) South Atlantic across the deglaciation (MD07-3076; Fig. 6a; Skinner et al., 2013). This offset of GL1090 to less radiogenic values than MD07-3076 suggests that the mid-depth South Atlantic was bathed by a greater proportion of NSW than the deep South Atlantic throughout the deglaciation. The neodymium isotope gradient between the mid-depth (i.e., GL1090) and deep (i.e., MD07-3076) South Atlantic suggests that there was a sustained presence of NSW in the mid-depth Atlantic throughout the past 25 kyr.

The deglacial trends in ε_{Nd} throughout the South Atlantic are notably different from those in benthic foraminiferal $\delta^{13}C$ from the same cores (Fig. 6b). The $\delta^{13}C$ of the mid-depth South Atlantic shifts to lower values from the LGM to HS1 when the ε_{Nd} values show little to no shift, indicating a clear decoupling between ε_{Nd} and $\delta^{13}C$. Furthermore, during HS1, although GL1090 at 2225 m exhibits the least radiogenic ε_{Nd} values of all four sites (Fig. 6a), suggesting the greatest proportion of NSW, it displays $\delta^{13}C$ values that are 0.2 - 0.5‰ lower than the shallower southern Brazil margin cores (Fig. 6b). Like the ε_{Nd} records, the $\delta^{13}C$ records from the South and North Atlantic mid-depth cores (i.e., GL1090 and SU90-03) appear similar throughout most of the past 25 kyr (Fig. 5); however, the lower deglacial resolution of the $\delta^{13}C$ record of GL1090 compared to SU90-03 reduces the certainty of this observation. Notwithstanding this issue of temporal resolution, lower LGM than Holocene $\delta^{13}C$ values are observed in both cores, which is consistent with a greater fraction of SSW during the LGM, as also suggested by the ε_{Nd} records.

Although small, the shift of the authigenic ε_{Nd} record of GL1090 to ~0.5 less radiogenic ε unit values around 18 ka is outside of analytical error (Fig. 3b). This slight unradiogenic excursion could represent a shift in the northern-sourced end-member, a hypothesis supported by a similar excursion in an intermediate depth ε_{Nd} record from the overflows of the Nordic Seas (Crocker et al., 2016), or they could instead represent a transient shift in the depth of the water mass mixing boundary between GNAIW and the mixture of GNADW and GAABW below (Curry and Oppo, 2005; Howe et al., 2016). Testing this possibility would require both a higher resolution record of the end-member composition from the North Atlantic as well as extension of the GL1090 ε_{Nd} record further back into the glacial period to examine whether there were more such excursions and whether they have any correlation to other Heinrich Stadials.

3.3 Atlantic water mass provenance: LGM vs. HS1

The South Atlantic LGM and HS1 profiles of ε_{Nd} and $\delta^{13}C$ (Fig. 7) are significantly different from one another, providing new constraints on water mass provenance and the carbon cycle within the South Atlantic at these times. The ε_{Nd} values for the South Atlantic are within error of one another for the LGM and HS1, suggesting no change in water mass provenance assuming constant end-members (Fig. 7a). In both profiles (Fig. 7a) GL1090 at 2225 m depth exhibits the least radiogenic ε_{Nd} values, suggesting that the greatest proportion of NSW occurred at mid-depths. The LGM $\delta^{13}C$ profile is exhibits a slightly shallower maximum around 1700 m, likely due to high $\delta^{13}C$ Glacial North Atlantic Intermediate Water (GNAIW) (Fig. 7b) (Curry and Oppo, 2005; Sarnthein et al., 1994). Unlike ε_{Nd}, however, the $\delta^{13}C$ profile for HS1 is significantly different from that of the LGM; the $\delta^{13}C$ values of the mid-depth South Atlantic in the HS1 profile are much lower. Furthermore, the HS1 profile shows decreasing $\delta^{13}C$ values with increasing depth below ~1700 m. It is important to note that the benthic $\delta^{13}C$ values do not all come from the same species and that the possibility of the Mackensen effect causing lower than seawater values to be preserved must be considered (Mackensen et al., 1993). This is particularly important when considering the low values exhibited by *Cibicidoides kullenbergi* from MD07-3076, although such low values have been reported at similar depths across the glacial South Atlantic (Waelbroeck et al., 2011).

Our new meridional sections of Atlantic ε_{Nd} constructed by combining the new data presented in this work with suitable published data (Fig. 8) support our hypothesis that the South Atlantic mid-depth water mass provenance was similar during the LGM and HS1. The ε_{Nd} sections of the Atlantic during the LGM and HS1 are very similar (Fig. 8); out of 22 cores for which both LGM and HS1 data are available 17 have values for the two time periods that are within error of each other (Table S7). The effect of age model uncertainty is minimal as many of the records exhibit negligible changes across the time period spanning all of the LGM and HS1. Therefore even shifting the age models by 1000 years would have little impact upon the sections shown in Fig. 8.

One region that does display a potentially significant difference is in the intermediate to mid-depth North Atlantic, which exhibits less radiogenic values during HS1 than during the LGM (Fig. 8, Table S7). However, the data are more sparse in this region during the LGM than HS1 due to complete lack of coral measurements from the LGM (Wilson et al., 2014). The unradiogenic coral results from HS1 are within error of the composition of upper Labrador Sea Water in the modern ocean (Lambelet et al., 2016; Wilson et al., 2014), therefore do not require an end-member change relative to the modern ocean, but due to the lack of glacial data the end-member ε_{Nd} of GNAIW is harder to determine. As a result we cannot rule out the possibility that NSW was less radiogenic during HS1 than the LGM, as suggested by a recent simulation (Gu et al., 2017).

Constraining whether changes in the neodymium composition of the end-member water masses occurred between the LGM and HS1 is a key component of interpreting the similarity of the ε_{Nd} values of the mid-depth South Atlantic during these two time periods (Fig. 7a). The ε_{Nd} record of SU90-03 from the mid-depth North Atlantic is only around 0.5 ε unit less radiogenic during HS1 than the LGM (Fig. 5) suggesting any end-member shift between these time periods may have been small. However, SU90-03 was likely bathed by a mixture of NSW and SSW during the LGM (Curry and Oppo, 2005; Howe et al., 2016), therefore changes in northern-sourced endmember-composition could be obfuscated by changes in water mass mixing at the site. A foraminiferal ε_{Nd} record from site ODP 980 at 2168 m depth in the northernmost North Atlantic exhibits very similar values during the LGM and HS1 (Crocker et al., 2016), a finding that would also be consistent with similar end-member composition for NSW from the Nordic Seas during those two time periods. The Nordic Seas overflow are, however, only one component of NSW as evidenced by the fact that the ODP 980 record is more radiogenic than SU90-03 during the LGM and HS1, which reveals the lack of Labrador Sea Water at the overflow site. Intermediate depth corals from the North Atlantic exhibit variable values during HS1 (Wilson et al., 2014), suggesting that there may have been short term changes in the composition of NSW at those depths. Notwithstanding these possible slight fluctuations in the neodymium composition of NSW during HS1, based upon the results from SU90-03 and ODP 980 we estimate that the average HS1 composition of NSW was not more than 1 ε unit different to that during the LGM.

The end-member composition of AAIW during both the LGM and HS1 is very poorly constrained. The only intermediate depth ε_{Nd} reconstruction from the Atlantic sector of the Southern Ocean (Robinson and van de Flierdt, 2009) is not sampling true AAIW as discussed by Howe et al (2016a). While we cannot discount the possibility that AAIW in the South Atlantic may have been more radiogenic during the LGM and HS1 (Gu et al., 2017), we adopt the position of Howe et al (2016a) and infer that the stability of the ε_{Nd} records in the intermediate depth South Atlantic (Fig. 4) shows no evidence to suggest less radiogenic AAIW values during these time periods. Furthermore, despite this uncertainty, we are primarily interested in the difference between the LGM and HS1, therefore any possible gradual end-member change across the deglaciation need not affect our investigation of water mass mixing proportions for these two time periods. More ε_{Nd} reconstructions and seawater ε_{Nd} measurements in the intermediate depths of the Southern Ocean are needed to better constrain the change in the ε_{Nd} end-member composition of AAIW during the LGM and HS1, as well as the potential influence of boundary exchange (Lacan and Jeandel, 2005) in the Southern Ocean.

Assuming that any end-member shifts between the LGM and HS1 were indeed small, the similarity of the LGM and HS1 ε_{Nd} values suggest that the provenance of water masses in the intermediate to mid-depth South Atlantic was very similar during this period (Fig. 8). These considerations are captured in the cross plots of $\delta^{13}C$ versus ε_{Nd} for HS1 and LGM (Fig. 9) constructed using the data from the five cores plotted in Figs. 5 and 6, revealing the apparent changes in end-member composition for both $\delta^{13}C$ and ε_{Nd} estimated in this work. A significant decrease in the $\delta^{13}C$ of NSW is speculated along with higher $\delta^{13}C$ of southern-sourced intermediate depth water. The only significant change in ε_{Nd} end-member for which there is strong evidence is the variants of AABW in the deep South Atlantic (Fig. 9). Using these end-members, based on sensitivity calculations of end-member changes (Howe et al., 2016) we estimate that the proportion of NSW in the mid-depth South Atlantic is unlikely to have decreased by more than 15% between the LGM and HS1. This decrease is consistent with estimates based upon benthic foraminiferal oxygen isotopes from the mid-depth South Atlantic (Lund et al., 2015) but significantly less than the 60% decrease that is needed if a greater proportion of SSW alone was responsible for the $\delta^{13}C$ decrease in the mid-depth Atlantic during HS1 (Oppo et al., 2015).

The lack of change in the ε_{Nd} profiles between the LGM and HS1 in the mid-depth South Atlantic (Fig. 5a) therefore indicates that the lower $\delta^{13}C$ values in HS1 than during the LGM observed at mid-depths (Fig. 5b) cannot be due to a greater proportion of low-$\delta^{13}C$ SSW and that NSW continued to influence the mid-depth South Atlantic during HS1. Thus we conclude that, contrary to the accepted paradigm (Keigwin and Lehman, 1994), the LGM to HS1 $\delta^{13}C$ decrease in the mid-depth South Atlantic is not due to the presence of a greater fraction of SSW (Oppo and Curry, 2012).

To reconcile our finding that the proportion of NSW and SSW masses were similar during the LGM and HS1 with evidence of an extremely weak or collapsed Atlantic overturning circulation in the mid-depth (Mulitza et al., 2017) and deep ocean (McManus et al., 2004), we propose that the production of NSW and at least some component of SSW were coupled. Accordingly, as the production of GNAIW weakened at the beginning of HS1, presumably due to the discharge of icebergs to the North Atlantic (Hemming, 2004), the production of some portion of SSW, here we suggest AAIW, may have decreased proportionately. There is strong evidence for better ventilation of the Southern Ocean during HS1 than during the LGM (e.g., Anderson et al., 2009; Burke and Robinson, 2012; Skinner et al., 2010). Such evidence is commonly taken as support for the bipolar seesaw hypothesis (Broecker, 1998) from which it is often assumed that the reduction in GNAIW formation during HS1 leads to greater SSW formation. We propose that whilst there may be an increase in AABW formation coincident with the increased ventilation of the deep Southern Ocean and South Atlantic (Burke and Robinson, 2012; Skinner et al., 2010) that the same may not be true for AAIW. Although still debated (e.g. the export of AAIW to the intermediate depths of the Caribbean Sea was strong during late HS1, Poggemann et al., 2017;

Valley et al., 2017), there is increasing evidence that AAIW did not penetrate significantly further north in the Atlantic during HS1 (Howe et al., 2016a; Huang et al., 2014; Xie et al., 2014). This evidence is consistent with a recent deglacial transient simulation performed with a neodymium-enabled ocean model (Gu et al., 2017). Furthermore, as AAIW is formed north of the Polar Front whereas AABW is formed through shelf processes and deep convection south of the Polar Front (Meredith et al., 1999) the two processes need not be intrinsically linked. Therefore, we suggest that AAIW formation may have decreased in concert with a decrease in GNAIW formation at the start of HS1 despite a potential increase in AABW production due to the bipolar seesaw (Broecker, 1998). This proposed decoupling of AAIW and AABW formation and the proportionate decrease in AAIW coupled to GNAIW formation would explain how the provenance of water in the mid-depth South Atlantic was able to remain similar during the LGM and HS1 despite an inferred lower rate of NSW formation (McManus et al., 2004).

The absence of a notable ε_{Nd} change in association with the LGM to HS1 decrease in $\delta^{13}C$ throughout the intermediate to mid-depth Atlantic argues against any explanation for the $\delta^{13}C$ decreases that involves a significantly greater proportion of SSW (Keigwin and Lehman, 1994; Oppo and Curry, 2012). Instead, changes in endmember $\delta^{13}C$ values or carbon cycling must have occurred (Lund et al., 2015; Oppo et al., 2015; Schmittner and Lund, 2015), creating a NSW mass with low $\delta^{13}C$ values. There is an increasing body of evidence from a number of different paleoceanographic proxies suggesting that the shift of NSW to significantly lower $\delta^{13}C$ values from the LGM to HS1 is likely explained by the greater accumulation of respired organic matter in poorly ventilated mid-depth waters (Böhm et al., 2015; Lacerra et al., 2017; McManus et al., 2004; Schmittner and Lund, 2015; Voigt et al., 2017). The effect of more sluggish circulation on $\delta^{13}C$ during HS1 may have been further enhanced by a greater supply of nutrients to the low latitudes during this time period (Poggemann et al., 2017). There are also other possible factors that may have contributed to the decrease in $\delta^{13}C$ in the mid-depth South Atlantic from the LGM to HS1 that, based on our results, may have occurred largely without changes in water mass mixing proportions. One of these is the release of low $\delta^{13}C$ deep water masses to the ocean interior or thermocline during HS1; this hypothesis, however, would be difficult to reconcile with the water mass end-members inferred from the cross plot of the data presented in this work for the LGM and HS1 (Fig. 9) as they do not appear to be consistent with low $\delta^{13}C$ values for AAIW during HS1. We note that, as discussed earlier, considerable uncertainty remains in the determination of the glacial end-members and the assignments are indeed speculative, therefore this hypothesis cannot be ruled out. An additional explanation for the low $\delta^{13}C$ during HS1 could be that rather than changes in the circulation rate or rate of supply of nutrients the remineralisation rate of organic matter in the ocean interior may have been higher (Kwon et al., 2009).

Our results cannot distinguish between changes in flow speed, nutrient supply/rain rate, or remineralisation rate; nor can they distinguish water mass advection from diffusion along isopycnals. However, whatever the mechanism, we suggest that the similarity of $\delta^{13}C$ values in the North and South Atlantic during HS1 (Oppo and Curry, 2012; Thiagarajan et al., 2014) was likely due to an apparent NSW end-member shift to lower $\delta^{13}C$ values counterbalanced by a shift of intermediate depth SSW to more positive values than during the LGM (Oppo et al., 2015). Furthermore, the ε_{Nd} results from GL1090 suggest that NSW influenced the mid-depth South Atlantic during HS1 (Fig. 8). This conclusion is a fundamental advance in both the understanding of how ocean circulation responds to sudden perturbations, such as potential freshwater forcing, and of the relationship between Atlantic overturning and the climate across millennial scale climate events.

4. Conclusions

We present two new foraminiferal ε_{Nd} records from the mid-depth South Atlantic. The deeper, and slightly more northerly, site shows consistently less radiogenic values and the sustained influence of northern-sourced waters throughout the deglaciation. Both sites display similar ε_{Nd} values during the LGM and HS1, suggesting that there were similar water mass mixing proportions at these times, despite significantly lower $\delta^{13}C$ values during HS1 than the LGM at the same sites. Consistent with other recent studies, we infer that this low $\delta^{13}C$ was primarily caused by greater accumulation of respired organic matter in the mid-depth North Atlantic due to significantly weakened circulation during HS1, possibly coupled with lower northern-sourced water $\delta^{13}C$, although we note that our results cannot discount other mechanisms that may have contributed to the low $\delta^{13}C$ values. Our results do, however, highlight the strength of combining $\delta^{13}C$ and ε_{Nd} data to investigate past changes in overturning circulation. Furthermore, the compilation of Atlantic ε_{Nd} data for the LGM and HS1 suggests little change in ε_{Nd} values in the Atlantic between those two time periods, indicating that the collapse in Atlantic overturning ascribed to HS1 caused little change in water mass mixing proportions in the Atlantic. As a result, we conclude that if freshwater forcing decreased the rate of formation of northern-sourced waters in the Atlantic at the onset of HS1 then the formation of intermediate-depth southern-sourced waters must also have decreased approximately in proportion.

Acknowledgements:

Ana Luiza S. Albuquerque is thanked for providing core material from GL1090. Vicky Rennie, KR Pietro, Jo Clegg, Jason Day, Mervyn Greaves and Caroline Daunt are thanked for technical support and Thiago Pereira dos Santos is thanked for providing stable isotope data from GL1090. Nd isotope analyses were supported by NERC grants NE/K005235/1 and NE/F006047/1 to AMP and NSF Grant OCE-1335191 to DWO. DWO acknowledges funding from WHOI's investment in Science Program. KFH acknowledges financial support from Academia Sinica and Taiwan MOST (MOST 104-2628-M-001-007-MY3). CMC acknowledges financial support from FAPESP (grant 2012/17517-3) and CAPES (grants 1976/2014 and 564/2015), and SM was supported by the DFG Research Center/Cluster of Excellence "The Ocean in the Earth System".

Figures/Tables:

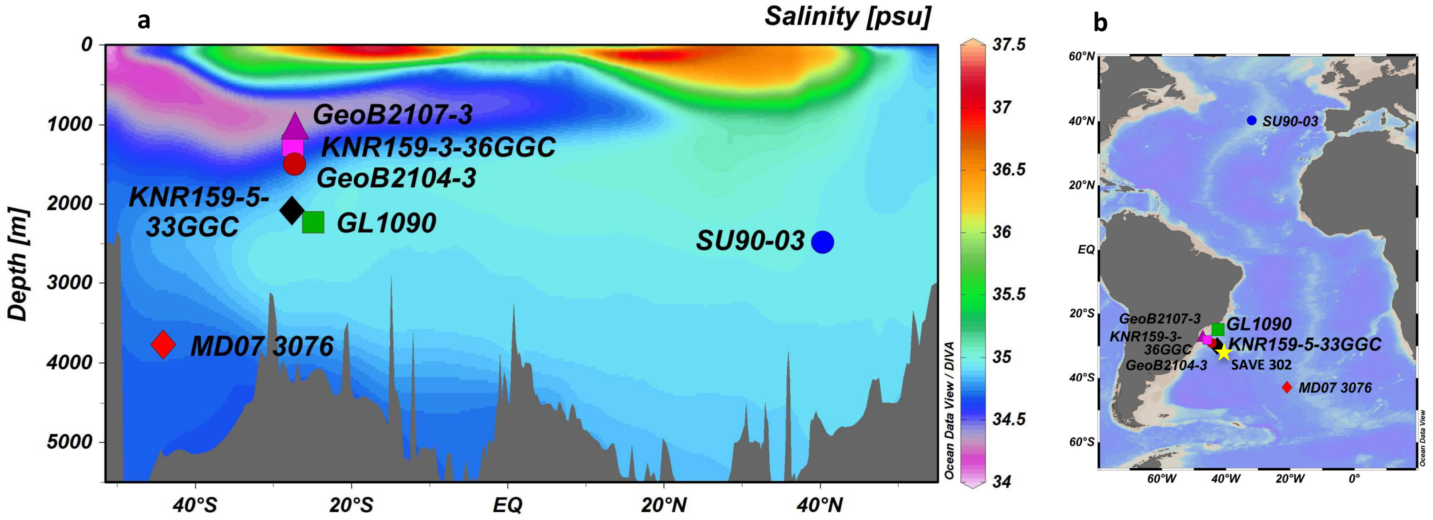

Fig. 1: (a) Salinity section of the western Atlantic (Antonov et al., 2010) showing the location of the cores used in this work, KNR159-5-33GGC (27.6°S, 46.2°W, 2082 m) and GL1090 (24.9°S, 42.5°W, 2225 m) along with core sites from which published ε_{Nd} records are discussed. Core locations and data references for all records are given in Table S1. (b) Map showing the locations of the cores present in panel a. The location of the station SAVE 302 by Jeandel (1993) is also indicated (yellow star). Both figures were produced using the Ocean Data View software (Schlitzer, 2016).

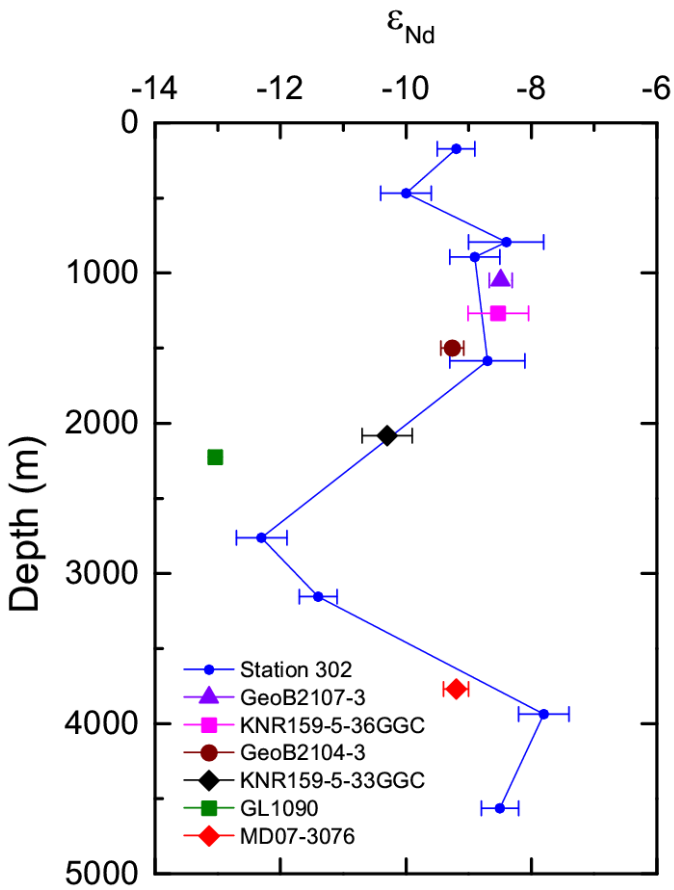

Fig. 2 Comparison of core top foraminiferal ε_{Nd} of cores KNR159-5-33GGC and GL1090 from the Brazil margin measured in this work along with core top values from nearby intermediate depth sites (GeoB2107-3, KNR159-5-36GGC and GeoB2104-3; Howe et al., 2016a) and a site from the Mid-Atlantic Ridge (MD07-3076; Skinner et al., 2013) compared to nearby seawater ε_{Nd} (SAVE 302, 33.6°S, 41.6°W; Jeandel, 1993). Note that all core top samples are younger than 5 ka, with the exception of the sample from GL1090 that shows an age of 6.8 ka.

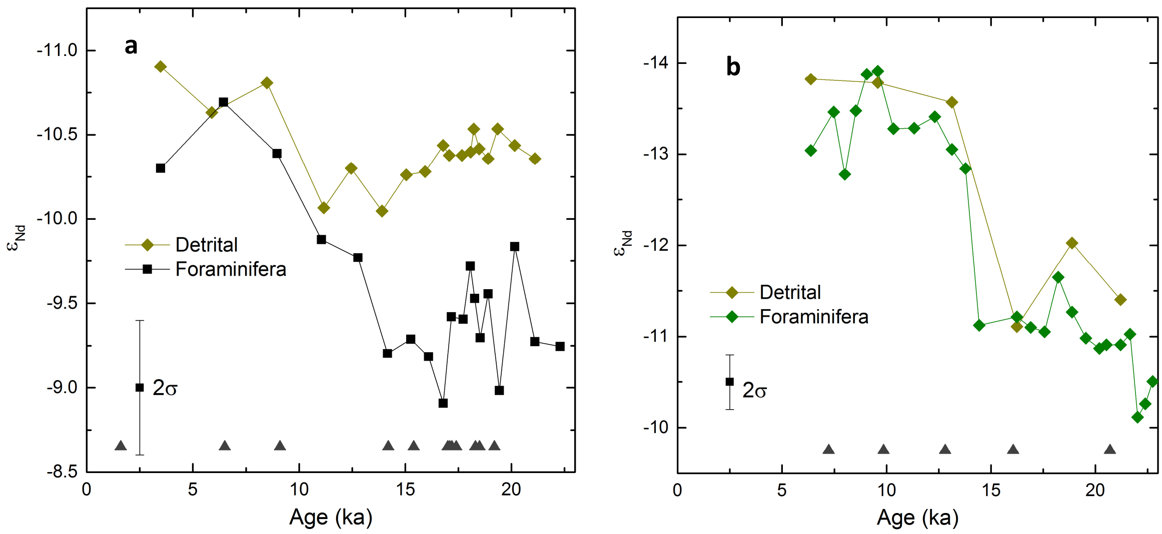

Fig. 3. Detrital (gold diamonds) and foraminiferal (black squares and green diamonds) ε_{Nd} of cores **(a)** KNR159-5-33GGC and **(b)** GL1090 with average 2σ error of all measurements plotted. Age control tie points are given by grey triangles on both plots.

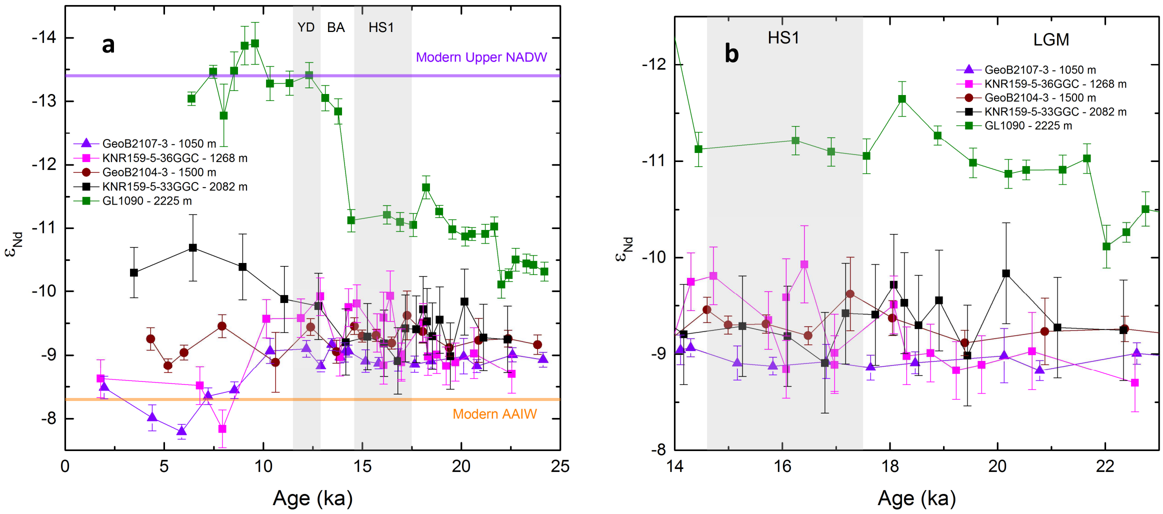

Fig. 4. (a) ε_{Nd} of uncleaned planktic foraminifera records of the past 25 kyr from KNR159-5-33GGC (black) and GL1090 (green) compared with those of GeoB2107-3 (purple), KNR159-5-36GGC (pink) and GeoB2104-3 (burgundy). Also labelled are the ε_{Nd} of modern Upper North Atlantic Deep Water (NADW) (-13.4; Lambelet et al., 2016) and Antarctic Intermediate Water (AAIW) (-8.3; Stichel et al., 2012). (b) Magnification of the LGM to HS1 period of all 5 cores. Climate periods labelled are the Younger Dryas (YD), Bølling-Allerød (BA) and Heinrich Stadial 1 (HS1). Core locations and data references for all records are given in Table S1.

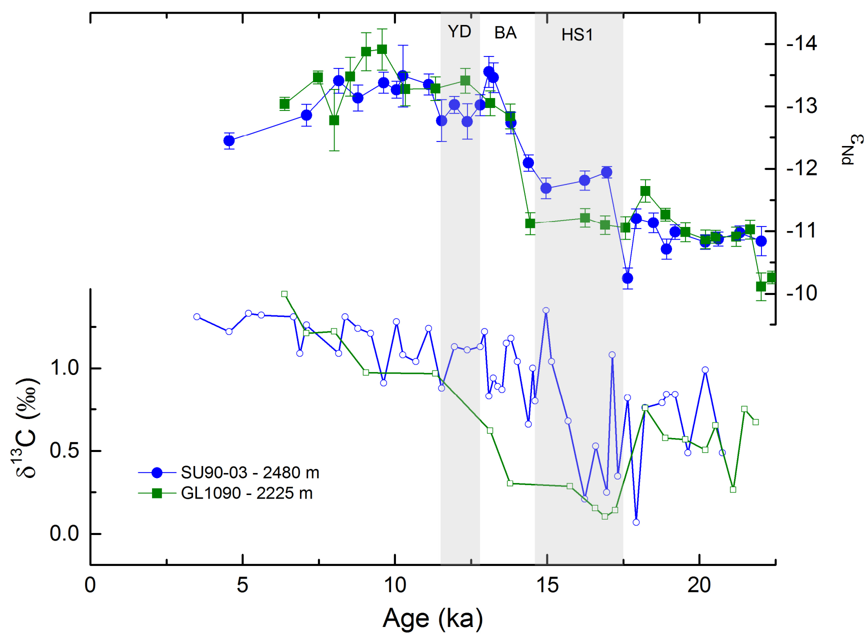

Fig. 5. (Top) ε_{Nd} of uncleaned planktic foraminifera from GL1090 (filled green squares) and SU90-03 (filled blue circles; Howe et al., 2016b). Benthic foraminiferal $\delta^{13}C$ measured on *Cibicidoides wuellerstorfi* from GL1090 (hollow green squares; Santos et al., 2017) and SU90-03 (hollow blue circles; Chapman and Shackleton, 1998). Climate periods labelled are the Younger Dryas (YD), Bølling-Allerød (BA) and Heinrich Stadial 1 (HS1).

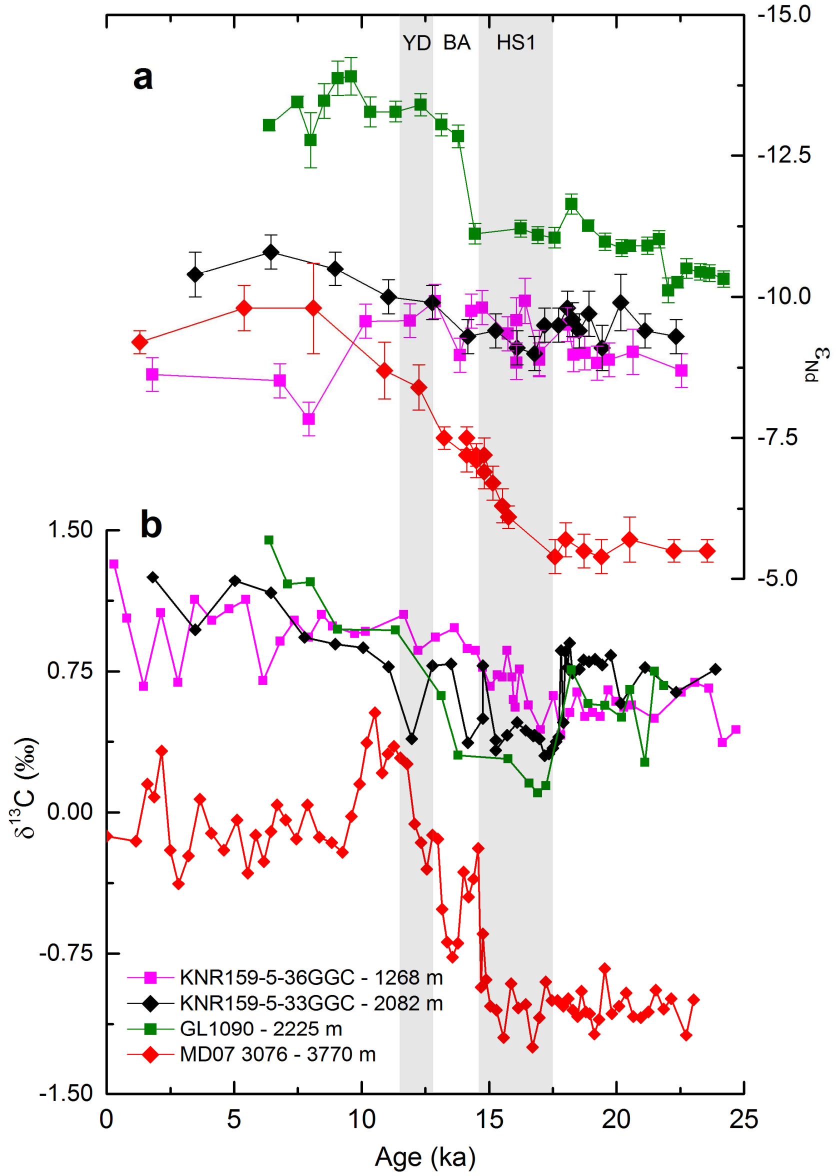

Fig. 6. (a) ε_{Nd} of uncleaned planktic foraminifera from cores KNR159-5-36GGC (pink; Howe et al., 2016a) KNR159-5-33GGC (black) and GL1090 (green), together with uncleaned benthic foraminifera of core MD07-3076 (red; Skinner et al., 2013). **(b)** Benthic foraminiferal $\delta^{13}C$ of mixed *Cibicidoides* and *Planulina* species from KNR159-5-36GGC (pink; Curry and Oppo, 2005) mixed *Cibicidoides* species from KNR159-5-33GGC (black; Tessin and Lund, 2013), *Cibicidoides wuellerstorfi* from GL1090 (green; Santos et al., 2017) and *Cibicides kullenbergi* from MD07-3076 (red; Waelbroeck et al., 2011). Climate periods labelled are the Younger Dryas (YD), Bølling-Allerød (BA) and Heinrich Stadial 1 (HS1). Core locations are given in Fig. 1.

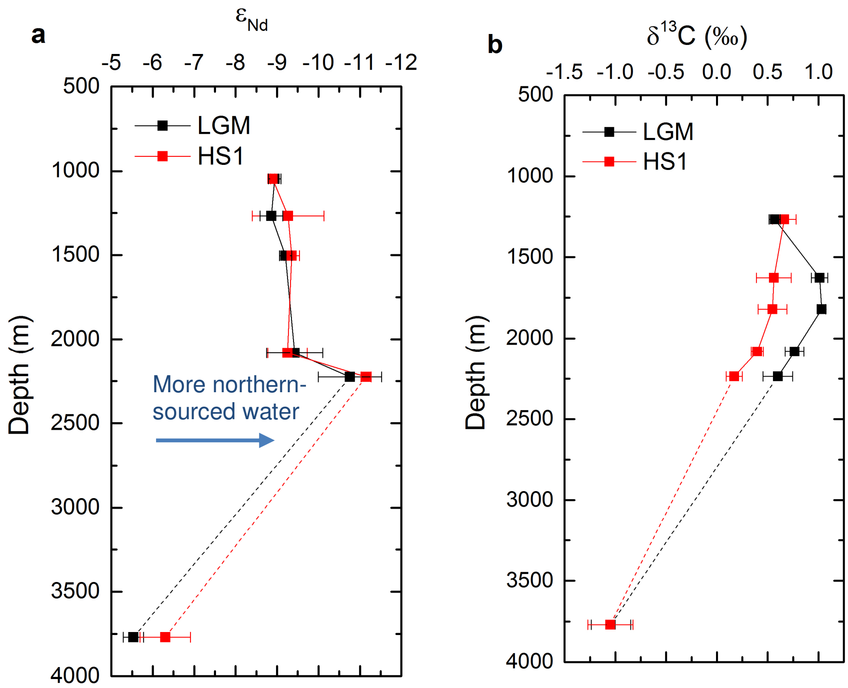

Fig. 7. Profiles of (**a**) authigenic ε_{Nd} and (**b**) benthic foraminiferal $\delta^{13}C$ of the Last Glacial Maximum (LGM) (23-19 ka) and Heinrich Stadial 1 (HS1) (17.5-15 ka) for the South Atlantic. ε_{Nd} data comes from refs. (Howe et al., 2016a; Skinner et al., 2013) and this work. $\delta^{13}C$ data comes from refs. (Curry and Oppo, 2005; Santos et al., 2017; Tessin and Lund, 2013; Waelbroeck et al., 2011) and are listed in Table S7.

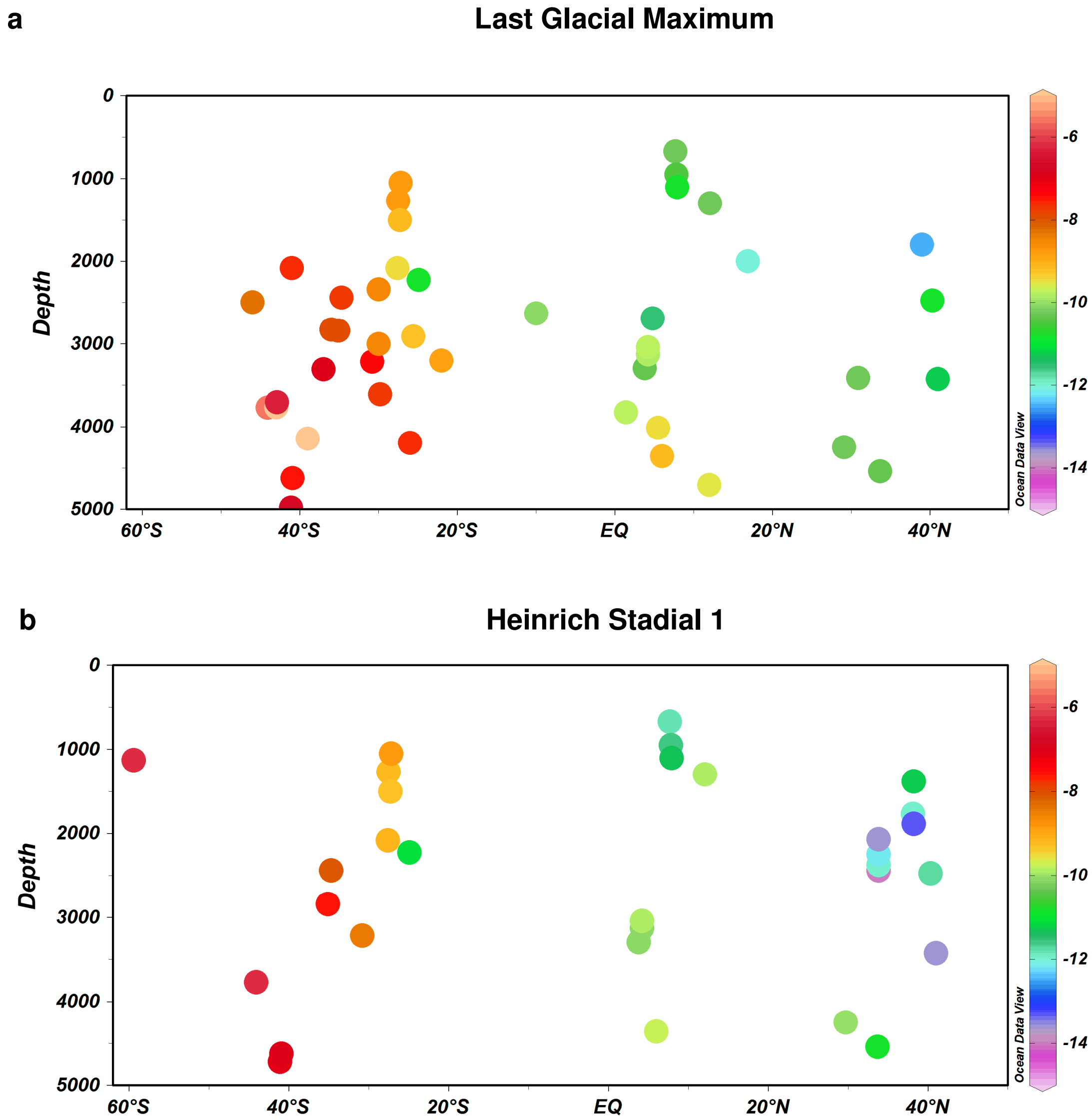

Fig. 8. Sections of authigenic ε_{Nd} from the western Atlantic, including the Mid-Atlantic Ridge, as well as the Cape Basin and the Drake Passage, for (a) the Last Glacial Maximum (23-19 ka) and (b) Heinrich Stadial 1 (17.5-15 ka). Core/site locations and names along with individual references are given in Fig. S2 and Tables S4 and S5. Sections were produced using the Ocean Data View software (Schlitzer, 2016).

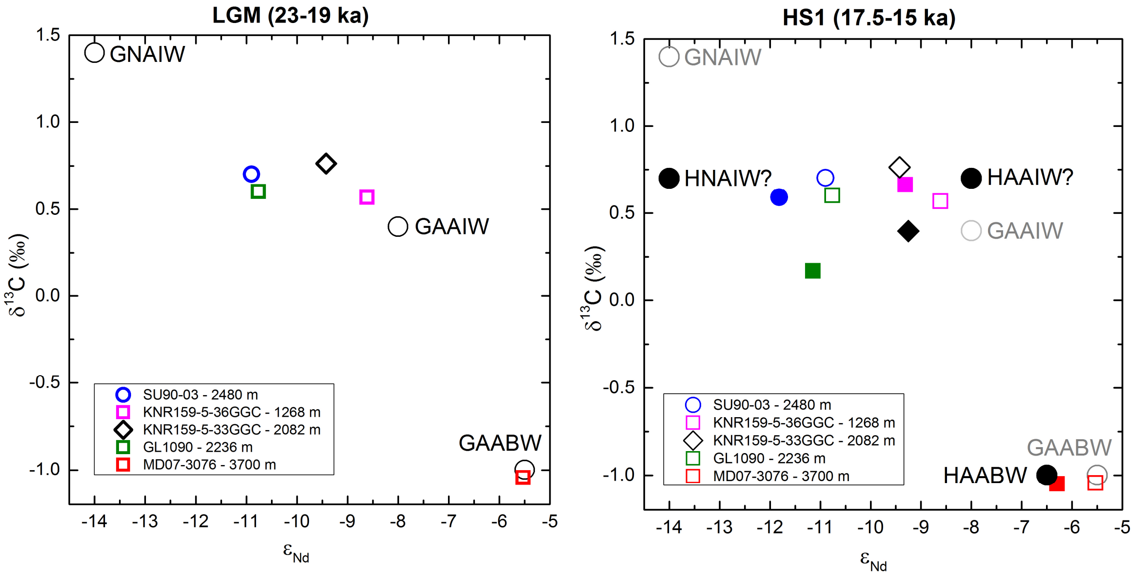

Fig. 9. Cross plots of authigenic ε_{Nd} versus benthic foraminiferal $\delta^{13}C$ for cores SU90-03, KNR159-5-36GGC, KNR159-5-33GGC, GL1090 and MD07-3076 during the Last Glacial Maximum (LGM) (23-19 ka; hollow symbols shown in both panels) and Heinrich Stadial 1 (HS1) (17.5-15 ka; filled symbols). Data points are averages for each of the time periods, taken from the records and references in Figs. 4 and 5. Endmembers labelled are Glacial (G) and Heinrich Stadial 1 (H) North Atlantic Intermediate Water (NAIW), Antarctic Intermediate Water (AAIW) and Antarctic Bottom Water (AABW).

References:

Anderson, R.F., Ali, S., Bradtmiller, L.I., Nielsen, S.H.H., Fleisher, M.Q., Anderson, B.E., Burckle, L.H., 2009. Wind-driven upwelling in the Southern Ocean and the deglacial rise in atmospheric CO_2. Science 323, 1443–1448.

Antonov, J.I., Seidov, D., Boyer, T.P., Locarnini, R.A., Mishonov, A. V., Garcia, H.E., Baranova, O.K., Zweng, M.M., Johnson, D.R., 2010. World Ocean Atlas 2009, Volume 2: Salinity. U.S. Government Printing Office.

Bayon, G., German, C.R., Boella, R.M., Milton, J.A., Taylor, R.N., Nesbitt, R.W., 2002. An improved method for extracting marine sediment fractions and its application to Sr and Nd isotopic analysis. Chem. Geol. 187, 179 – 199.

Böhm, E., Lippold, J., Gutjahr, M., Frank, M., Blaser, P., Antz, B., Fohlmeister, J., Frank, N., Andersen, M.B., Deininger, M., 2015. Strong and deep Atlantic meridional overturning circulation during the last glacial cycle. Nature 517, 73–76. doi:10.1038/nature14059

Boiteau, R., Greaves, M., Elderfield, H., 2012. Authigenic uranium in foraminiferal coatings: A proxy for ocean redox chemistry. Paleoceanography 27, PA3227. doi:10.1029/2012PA002335

Bond, G. C., et al., 1992. Evidence for massive discharges of icebergs into the North Atlantic Ocean during the last glaciation. Nature 360, 245-249.

Boyle, E.A., Keigwin, L.D., 1987. North Atlantic thermohaline circulation during the past 20,000 years linked to high-latitude surface temperature. Nature 330, 35–40.

Bradtmiller, L.I., McManus, J.F., Robinson, L.F., 2014. $^{231}Pa/^{230}Th$ evidence for a weakened but persistent Atlantic meridional overturning circulation during Heinrich Stadial 1. Nat. Commun. 5, 5817. doi:10.1038/ncomms6817

Broecker, W. S., 1994. Massive iceburg discharges as triggers for global climate change. Nature 372, 421-424.

Broecker, W.S., 1998. Paleocean circulation during the Last Deglaciation: A bipolar seesaw? Paleoceanography 13, 119–121. doi:10.1029/97PA03707

Burke, A., Robinson, L.F., 2012. The Southern Ocean's role in carbon exchange during the last deglaciation. Science 335, 557–61. doi:10.1126/science.1208163

Chapman, M.R., Shackleton, N.J., 1998. Millennial-scale fluctuations in North Atlantic heat flux during the last 150,000 years. Earth Planet. Sci. Lett. 159, 57–70.

Chapman, M.R., Shackleton, N.J., Duplessy, J.-C., 2000. Sea surface temperature variability during the last glacial-interglacial cycle: assessing the magnitude and pattern of climate change in the North Atlantic. Palaeogeogr. Palaeoclimatol. Palaeoecol. 157, 1–25.

Crocker, A.J., Chalk, T., Bailey, I., Spencer, M.R., Gutjahr, M., Foster, G.L., Wilson, P.A., 2016. Geochemical response of the mid-depth Northeast Atlantic Ocean to freshwater input during Heinrich events 1 to 4. Quat. Sci. Rev. 151, 236–254. doi:10.1016/j.quascirev.2016.08.035

Curry, W.B., Lohmann, G.P., 1983. Reduced advection into Atlantic Ocean deep eastern basins during last glaciation maximum. Nature 306, 577–580.

Curry, W.B., Oppo, D.W., 2005. Glacial water mass geometry and the distribution of $\delta^{13}C$ of ΣCO_2 in the western Atlantic Ocean. Paleoceanography 20, PA1017. doi:10.1029/2004PA001021

De Mahiques, M.M., Tassinari, C.C.G., Marcolini, S., Violante, Roberto A. Figueira, R.C.L., Silveira, I.C.A. da, Burone, L., Sousa, S.H. de M. e, 2008. Nd and Pb isotope signatures on the Southeastern South American upper margin: Implications for sediment transport and source rocks. Mar. Geol. 250, 61–63.

Duplessy, J.C., Shackleton, N.J., Fairbanks, R.G., Labeyrie, L., Oppo, D.W., Kallel, N., 1988. Deepwater source variations during the last climatic cycle and their impact on the global deepwater circulation. Paleoceanography 3, 343–360.

Foster, G.L., Vance, D., Prytulak, J., 2007. No change in the neodymium isotope composition of deep water exported from the North Atlantic on glacial-interglacial time scales. Geology 35, 37–40. doi:10.1130/G23204A.1

Frank, M., 2002. Radiogenic isotopes: tracers of past ocean circulation and erosional input. Rev. Geophys. 40. do1:10.1029/2000RG000094.

Garcia-Solsona, E., Jeandel, C., Labatut, M., Lacan, F., Vance, D., Chavagnac, V., Pradoux, C., 2014. Rare earth elements and Nd isotopes tracing water mass mixing and particle-seawater interactions in the SE Atlantic. Geochim. Cosmochim. Acta 125, 351–372. doi:10.1016/j.gca.2013.10.009

Gherardi, J., Labeyrie, L., Mcmanus, J., Francois, R., Skinner, L., Cortijo, E., 2005. Evidence from the Northeastern Atlantic basin for variability in the rate of the meridional overturning circulation through the last deglaciation. Earth Planet. Sci. Lett. 240, 710–723. doi:10.1016/j.epsl.2005.09.061

Goldstein, S. L., Hemming, S. R., 2003. Long lived isotopic tracers in oceanography, paleoceanography and ice-sheet dynamics. in Treatise Geochemistry, vol. 6.17, pp. 453-489, Elsevier, N. Y.

Gu, S., Liu, Z., Zhang, J., Rempfer, J., Joos, F., Oppo, D. W., 2017. Cohence response of Antarctic Intermediate Water and Atlantic Meridional Overturning Circulation during the last deglaication: reconciling contrasting neodymium isotope reconstructions in tropical Atlantic. Paleoceanography 32, 1036-1053.

Gutjahr, M., Frank, M., Stirling, C.H., Keigwin, L.D., Halliday, A.N., 2008. Tracing the Nd isotope evolution of North Atlantic Deep and Intermediate Waters in the western North Atlantic since the Last Glacial Maximum from Blake Ridge sediments. Earth Planet. Sci. Lett. 266, 61–77. doi:10.1016/j.epsl.2007.10.037

Hamilton, P.J., O'Nions, R.., Bridgwater, D., Nutman, A., 1983. Sm-Nd studies of Archaean metasediments and metavolcanics from West Greenland and their implications for the Earth's early history. Earth Planet. Sci. Lett. 62, 263–272.

Heil, G., 2006. Abrupt climate shifts in the western tropical to subtropical Atlantic region during the last glacial. Bremen University.

Hemming, S.R., 2004. Heinrich events: Massive late Pleistocene detritus layers of the North Atlantic and their global climate imprint. Rev. Geophys. 42, RG1005. doi:10.1029/2003RG000128.1.

Hickey, B., 2010. Reconstructing past flow rates of southern component water masses using sedimentary ^{231}Pa/^{230}Th. University of Oxford.

Howe, J.N.W., Piotrowski, A.M., Noble, T.L., Mulitza, S., Chiessi, C.M., Bayon, G., 2016. North Atlantic Deep Water production during the Last Glacial Maximum. Nat. Commun. 7, 1–8. doi:10.1038/ncomms11765

Howe, J.N.W., Piotrowski, A.M., Oppo, D.W., Huang, K., Mulitza, S., Chiessi, C.M., Blusztajn, J., 2016a. Antarctic intermediate water circulation in the South Atlantic over the past 25,000 years. Paleoceanography 1–13. doi:10.1002/2016PA002975.

Howe, J.N.W., Piotrowski, A.M., Rennie, V.C.F., 2016b. Abyssal origin for the early Holocene pulse of unradiogenic neodymium isotopes in Atlantic seawater. Geology 831, 831–834. doi:10.1130/G38155.1

Huang, K.-F., Blusztajn, J., Oppo, D.W., Curry, W.B., Peucker-Ehrenbrink, B., 2012. High-precision and accurate determinations of neodymium isotopic compositions at nanogram levels in natural materials by MC-ICP-MS. J. Anal. At. Spectrom. 27, 1560. doi:10.1039/c2ja30123g

Huang, K.-F., Oppo, D.W., Curry, W.B., 2014. Decreased influence of Antarctic intermediate water in the tropical Atlantic during North Atlantic cold events. Earth Planet. Sci. Lett. 389, 200–208. doi:10.1016/j.epsl.2013.12.037

Jacobsen, S.B., Wasserburg, G.J., 1980. Sm-Nd isotopic evolution of chondrites. Earth Planet. Sci. Lett. 50, 139–155.

Jeandel, C., 1993. Concentration and isotopic composition of Nd in the South Atlantic Ocean. Earth Planet. Sci. Lett. 117, 581–591.

Jonkers, L., Zahn, R., Thomas, A., Henderson, G., Abouchami, W., François, R., Masque, P., Hall, I.R., Bickert, T., 2015. Deep circulation changes in the central South Atlantic during the past 145 kyrs reflected in a combined $^{231}Pa/^{230}Th$, Neodymium isotope and benthic $\delta^{13}C$ records. Earth Planet. Sci. Lett. 419, 14–21. doi:10.1016/j.epsl.2015.03.004

Keigwin, L.D., Lehman, S.J., 1994. Deep Circulation Change Linked to Heinrich Event-1 and Younger Dryas in a Middepth North-Atlantic Core. Paleoceanography 9, 185–194.

Kraft,S., Frank, M., Hathorne, E. C., Weldeab, S., 2013. Assessment of seawater Nd isotope signatures extracted from foraminiferal shells and authigenic phases of Gulf of Guinea sediments. Geochim. Cosmochim. Acta 121, 414-435.

Kwon, E.Y., Primeau, F., Sarmiento, J.L., 2009. The impact of remineralization depth on the air–sea carbon balance. Nat. Geosci. 2, 630–635. doi:10.1038/ngeo612

Lacan, F., Jeadel, C., 2005. Neodymium isotopes as a new tool for quantifiying exchange fluxes at the continent-ocean interface. Earth Planet. Sci. Lett. 232, 245-257.

Lacerra, M., Lund, D., Yu, J., Schmittner, A., 2017. Carbon storage in the min-depth Atlantic during millennial-scale climate events. Paleoceanography 1–16. doi:10.1002/2016PA003081

Lambelet, M., van de Flierdt, T., Crocket, K., Rehkämper, M., Kreissig, K., Coles, B., Rijkenberg, M.J.A., Gerringa, L.J.A., de Baar, H.J.W., Steinfeldt, R., 2016. Neodymium isotopic composition and concentration in the western North Atlantic Ocean: results from the GEOTRACES GA02 section. Geochim. Cosmochim. Acta 177, 1–29. doi:10.1016/j.gca.2015.12.019

Lang, D.C., Bailey, I., Wilson, P.A., Chalk, T.B., Foster, G.L., Gutjahr, M., 2016. Incursions of southern-sourced water into the deep North Atlantic during late Pliocene glacial intensification. Nat. Geosci. 9, 375–379. doi:10.1038/ngeo2688

Lantzsch, H., Hanebuth, T.J.J., Chiessi, C.M., Schwenk, T., Violante, R. a., 2014. The high-supply, current-dominated continental margin of southeastern South America during the late Quaternary. Quat. Res. 81, 339–354. doi:10.1016/j.yqres.2014.01.003

Lippold, J., Gutjahr, M., Blaser, P., Christner, E., Ferreira, M.L.D.C., Mulitza, S., Christl, M., Wombacher, F., Böhm, E., Antz, B., Cartapanis, O., Vogel, H., Jaccard, S.L., 2016. Deep water provenience and dynamics of the (de)glacial Atlantic meridional overturning circulation. Earth Planet. Sci. Lett. 445, 68–78. doi:10.1016/j.epsl.2016.04.013

Lund, D.C., Tessin, A.C., Hoffman, J.L., Schmittner, A., 2015. Southwest Atlantic water mass evolution during the last deglaciation. Paleoceanography 30. doi:10.1002/2014PA002657.

Mackensen, A., Hubberten, H., Bickert, T., Ftitterer, D.K., 1993. The $\delta^{13}C$ in benthic foraminifera tests of Fontbotia wuellerstorfi (Schwager) relative to the $\delta^{13}C$ of dissolved inorganic carbon in Southern Ocean deep water: implications for glacial ocean circulation models. Paleoceanography 8, 587–610.

Martin, E. E., Blair, S. W., Kamenov, G. D., Scher, H. D., Bourbon, E., Basak, C., Newkirk, D. N., 2010. Extraction of Nd isotopes from bulk deep sea sediments for paleoceanographic studies on Cenozoic time scales. Chem. Geol. 269, 414-431.

McManus, J.F., Francois, R., Gherardi, J.-M., Keigwin, L.D., Brown-Leger, S., 2004. Collapse and rapid resumption of Atlantic meridional circulation linked to deglacial climate changes. Nature 428, 834–837. doi:10.1038/nature02494

Meredith, M.P., Grose, K.E., McDonagh, E.L., Heywood, K.J., Frew, R.D., Dennis, P.F., 1999. Distribution of oxygen isotopes in the water masses of Drake Passage and the South Atlantic. J. Geophys. Res. 104, 20949–20962. doi:10.1029/98jc02544

Molina-Kescher, M., Frank, M., Hathorne, E. C., 2014. Nd and Sr isotope compositions of different phases of surface sediments in the South Pacific: Extraction of seawater signature, boundary exchnage, and detrital/dust provenance. Geochem. Geophys. Geosyst. 15, 3502-3520.

Mulitza, S., Chiessi, C. M., SchefuB, E., Lippold, J., Wichmann, D., Antz, B., Mackense, A., Paul, A., Prange, M., Rehfeld, K., Werner, M., Bickert, T., Frank, N., Kuhnert, H., Lynch-Stieglitz, J., Portilho-Ramos, R., Sawakuchi, A. O., Schulz, M., Schwenk, T., Tiedemann, R., Vahlenkamp, Zhang, Y., 2017. Synchronous and proportional deglaical changes in Atlantic meridional overturning and northeast Brazilian precipitation. Paleoceanography 32, 622-633. doi:10.1002/2017PA003084.

Neto, M., Figueiredo, M., 1995. The Rio Doce Orogeny, Southeastern Brazil. J. South Am. Earth Sci. 8, 143–162.

Oppo, D.W., Curry, W.B., 2012. Deep Atlantic circulation during the last glacial maximum and deglaciation. Nat. Educ. Knowl. 3.

Oppo, D.W., Curry, W.B., Mcmanus, J.F., 2015. What do benthic d13C and d18O data tell us about Atlantic circulation during Heinrich Stadial 1? Paleoceanography 30. doi:10.1002/2014PA002667.

Piepgras, D.J., Wasserburg, G.J., 1987. Rare earth element transport in the western North Atlantic inferred from Nd isotopic observations. Geochim. Cosmochim. Acta 51, 1257–1271. doi:10.1016/0016-7037(87)90217-1

Piotrowski, A.M., Galy, A., Nicholl, J.A.L., Roberts, N., Wilson, D.J., Clegg, J.A., Yu, J., 2012. Reconstructing deglacial North and South Atlantic deep water sourcing using foraminiferal Nd isotopes. Earth Planet. Sci. Lett. 357-358, 289–297.

Piotrowski, A.M., Goldstein, S.L., Hemming, S.R., Fairbanks, R.G., 2004. Intensification and variability of ocean thermohaline circulation through the last deglaciation. Earth Planet. Sci. Lett. 225, 205–220. doi:10.1016/j.epsl.2004.06.002

Poggemann, D., Hathorne, E.C., Nürnberg, D., Frank, M., Bruhn, I., Reißig, S., Bahr, A., 2017. Rapid deglacial injection of nutrients into the tropical Atlantic via Antarctic Intermediate Water. Earth Planet. Sci. Lett. 463, 118–126. doi:10.1016/j.epsl.2017.01.030

Reimer, P., Bard, E., Bayliss, A., Beck, J.W., Blackwell, P.G., Ramsey, C.B., Buck, C.E., Cheng, H., Edwards, R.L., Friedrich, M., Grootes, P.M., Guilderson, T.P., Haflidason, H., Hajdas, I., Hatté, C., Heaton, T.J., Hoffman, D.L., Hogg, A.G., Hughen, K.A., Kaise, K.F., Kromer, B., Manning, S.W., Niu, M., Reimer, R.W., Richard, D.A., Scott, E.M., Southon, J.R., Staff, R.A., Turney, C.S.M., Plicht, J. van der, 2013. IntCal13 and Marine13 Radiocarbon Age Calibration Curves 0–50,000 Years cal BP. Radiocarbon 55, 1869–1887. doi:10.2458/azu_js_rc.55.16947

Rickaby, R.E.M., Elderfield, H., 2005. Evidence from the high-latitude North Atlantic for variations in Antarctic Intermediate water flow during the last deglaciation. Geochemistry, Geophys. Geosystems 6, Q05001. doi:10.1029/2004GC000858

Rickli, J., Frank, M., Halliday, A.N., 2009. The hafnium–neodymium isotopic composition of Atlantic seawater. Earth Planet. Sci. Lett. 280, 118–127. doi:10.1016/j.epsl.2009.01.026

Roberts, N.L., Piotrowski, A.M., McManus, J.F., Keigwin, L.D., 2010. Synchronous deglacial overturning and water mass source changes. Science 327, 75–78. doi:10.1126/science.1178068

Robinson, L.F., van de Flierdt, T., 2009. Southern Ocean evidence for reduced export of North Atlantic Deep Water during Heinrich event 1. Geology 37, 195–198. doi:10.1130/G25363A.1

Santos, T.P., Lessa, D.O., Venancio, I.M., Chiessi, C.M., Mulitza, S., Kuhnert, H., Govin, A., Machado, T., Costa, K.B., Toledo, F., Dias, B.B., Albuquerque, A.L.S., 2017. Prolonged warming of the Brazil Current precedes deglaciations. Earth Planet. Sci. Lett. 463, 1-12.

Sarnthein, M., Winn, K., Jung, S.J.A., Duplessy, J.C., Labeyrie, L., Erlenkeuser, H., Ganssen, G., 1994. Changes in east Atlantic deepwater circulation over the last 30,000 years: Eight time slice reconstructions. Paleoceanography 9, 209–267.

Schlitzer, R., 2016. Ocean Data View [WWW Document]. URL http://odv.awi.de

Schmittner, A., Lund, D.C., 2015. Early deglacial Atlantic overturning decline and its role in atmospheric CO_2 rise inferred from carbon isotopes ($\delta^{13}C$). Clim. Past 11, 135–152. doi:10.5194/cp-11-135-2015

Skinner, L.C., Fallon, S., Waelbroeck, C., Michel, E., Barker, S., 2010. Ventilation of the deep Southern Ocean and deglacial CO2 rise. Science 328, 1147–1151. doi:10.1126/science.1183627

Skinner, L.C., Scrivner, A.E., Vance, D., Barker, S., Fallon, S., Waelbroeck, C., 2013. North Atlantic versus Southern Ocean contributions to a deglacial surge in deep ocean ventilation. Geology 41, 667–670. doi:10.1130/G34133.1

Sortor, R.N., Lund, D.C., 2011. No evidence for a deglacial intermediate water $\Delta^{14}C$ anomaly in the SW Atlantic. Earth Planet. Sci. Lett. 310, 65–72. doi:10.1016/j.epsl.2011.07.017

Stichel, T., Frank, M., Rickli, J., Haley, B.A., 2012. The hafnium and neodymium isotope composition of seawater in the Atlantic sector of the Southern Ocean. Earth Planet. Sci. Lett. 317-318, 282–294. doi:10.1016/j.epsl.2011.11.025

Tanaka, T., Togashi, S., Kamioka, H., Amakawa, H., Kagami, H., Hamamoto, T., Yuhara, M., Orihashi, Y., Yoneda, S., Shimizu, H., Kunimaru, T., Takahashi, K., Yanagi, T., Nakano, T., Fujimaki, H., Shinjo, R., Asahara, Y., Tanimizu, M., Dragusanu, C., 2000. JNdi-1: a neodymium isotopic reference in consistency with LaJolla neodymium. Chem. Geol. 168, 279–281. doi:10.1016/S0009-2541(00)00198-4

Taylor, S.R., McLennan, S., 1985. The Continental Crust: Its composition and evolution. Blackwell Scientific, Oxford. 312 pp.

Tessin, A.C., Lund, D.C., 2013. Isotopically depleted carbon in the mid-depth South Atlantic during the last deglaciation. Paleoceanography 28, 296–306. doi:10.1002/palo.20026

Thiagarajan, N., Subhas, A. V, Southon, J.R., Eiler, J.M., Adkins, J.F., 2014. Abrupt pre-Bølling-Allerød warming and circulation changes in the deep ocean. Nature 511, 75–8. doi:10.1038/nature13472

Thornalley, D.J.R., Elderfield, H., McCave, I.N., 2010. Intermediate and deep water paleoceanography of the northern North Atlantic over the past 21,000 years. Paleoceanography 25, 1–17. doi:10.1029/2009PA001833

Valley, S., Lynch-Stieglitz, J., Marchitto, T. M., 2017. Timing of deglacial AMOC variability from a high-resolution seawater cadmium reconstruction. Paleoceanography 32, 1195-1203.

Van de Flierdt, T., Robinson, L.F., Adkins, J.F., Hemming, S.R., Goldstein, S.L., 2006. Temporal stability of the neodymium isotope signature of the Holocene to glacial North Atlantic. Paleoceanography 21, PA4102. doi:10.1029/2006PA001294

Voigt, I., Cruz, A.P.S., Mulitza, S., Chiessi, C.M., Mackensen, A., Lippold, J., Antz, B., Zabel, M., Zhang, Y., Barbosa, C.F., Tisserand, A., 2017. Variability in mid-depth ventilation of the western Atlantic Ocean during the last deglaciation. Paleoceanography 32, 948-965.

Waelbroeck, C., Skinner, L.C., Labeyrie, L., Duplessy, J.-C., Michel, E., Vazquez Riveiros, N., Gherardi, J.-M., Dewilde, F., 2011. The timing of deglacial circulation changes in the Atlantic. Paleoceanography 26, PA3213. doi:10.1029/2010PA002007

Wei, R., Abouchami, W., Zahn, R., Masque, P., 2016. Deep circulation changes in the South Atlantic since the Last Glacial Maximum from Nd isotope and multi-proxy records. Earth Planet. Sci. Lett. 434, 18–29. doi:10.1016/j.epsl.2015.11.001

Wilson, D.J., Crocket, K.C., van de Flierdt, T., Robinson, L.F., Adkins, J.F., 2014. Dynamic intermediate ocean circulation in the North Atlantic during Heinrich Stadial 1: a radiocarbon and neodymium isotope perspective. Paleoceanography 29, 1072–1093. doi:10.1002/2014PA002674

Xie, R.C., Marcantonio, F., Schmidt, M.W., 2014. Reconstruction of intermediate water circulation in the tropical North Atlantic during the past 22,000 years. Geochim. Cosmochim. Acta 140, 455–467. doi:10.1016/j.gca.2014.05.041

Zahn, R., Stüber, A., 2002. Suborbital intermediate water variability inferred from paired benthic foraminiferal Cd/Ca and $\delta^{13}C$ in the tropical West Atlantic and linking with North Atlantic. Earth Planet. Sci. Lett. 200, 191–205.

Supplementary material:

Minor and Rare Earth Element Analyses

Calcium concentrations in the dissolved foraminiferal samples were measured using the Varian Vista inductively coupled optical emission spectrophotometer (ICP-OES) in the Department of Earth Sciences at the University of Cambridge. Samples were then diluted to 100 ppm calcium for minor and rare earth element analysis on the PerkinElmer SCIEX Elan DRC II Quadrupole inductively-coupled mass spectrometer. Samples were measured Al, Ca, Mn, U and the Rare Earth Elements. Analyses were performed by first measuring eight calibration standards, which spanned the range of typical foraminiferal concentrations, to produce a linear calibration curve. Samples were then run in blocks of ten bracketed by two additional standards with typical foraminiferal REE concentrations as consistency checks. Intensities were corrected for instrumental drift during the run using internal Rh, In and Re standards, and for oxide interferences. Results were converted to ppm calcium carbonate assuming 100% of calcium came from calcite; Rare Earth Element concentrations were then normalised to Post Archean Australian Shale (PAAS) (Taylor and McLennan, 1985).

Revised age model for SU90-03

The revised age model for core SU90-03 was constructed using a combination of AMS-^{14}C ages and lithological data (Chapman and Shackleton, 1998; Chapman et al., 2000). We adopted the AMS-^{14}C age control points for the Younger Dryas (at the depth of 40 cm, for 12 ka) and for the Last Glacial Maximum (at the depth of 121 cm, for 22.6 ka) from Chapman and Shackleton (1998) and Chapman et al. (2000), that were converted to calibrated ages using the R-package Bchron (Parnell et al., 2008) with the Marine13 calibration curve (Reimer et al., 2013). The prominent feature during Heinrich Stadial 1 based on the presence of ice rafted detritus lithic grains and the age for the end of HS1 (McManus et al., 2004) were used to provide additional age constraints for the deglaciation section of the core (at depths of 66 cm and 77 cm, for 14.7 and 16 ka, respectively). We then used the R-package Bchron (Parnell et al., 2008) with the Marine13 calibration curve (Reimer et al., 2013) to generate a core-top age of 3.5 ka. A comparison of the revised and the original (Chapman and Shakleton, 1998) age models is shown in Fig. S1, and the age-depth control points used in the revised version of the age model are listed below.

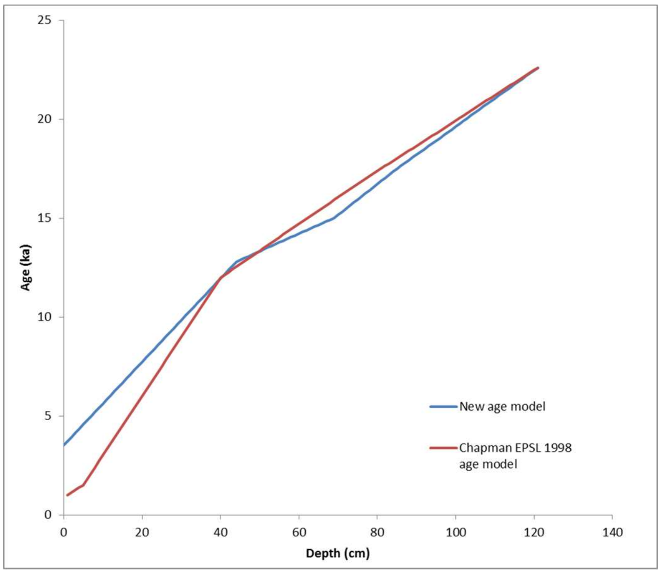

Fig. S1. A comparison of the age-depth model for core SU90-03 between the revised version used in this manuscript and its original version as published by Chapman and Shackleton (1998). Calibrated ages are used in the plot.

Age controls	Depth (cm)	^{14}C Age (ka)	Calendar age (ka)	Sources
BCHRON with MARINE13	0		3.5	
YD	40	10.5	12.0	Chapman and Shackleton (1998)
End of HS1	66		14.7	McManus et al (2004)
Peak IRD	77		16.0	
BCHRON with MARINE13	121	19.1	22.6	Chapman et al (2000)

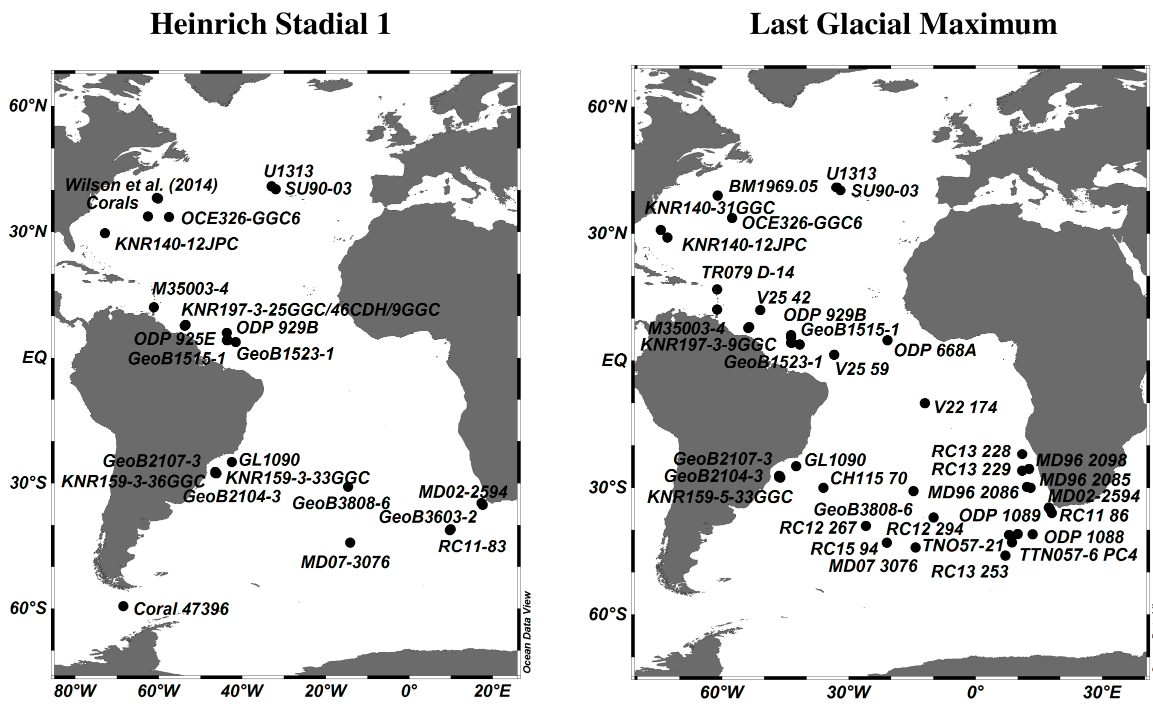

Fig. S2. Maps showing the location of cores and corals used for the reconstruction of ε_{Nd} values of the Atlantic during Heinrich Stadial 1 (left) and the Last Glacial Maximum (right). Complete core locations and data references are given in Tables S4 and S5. This figure was produced using the Ocean Data View software (Schlitzer, 2016).

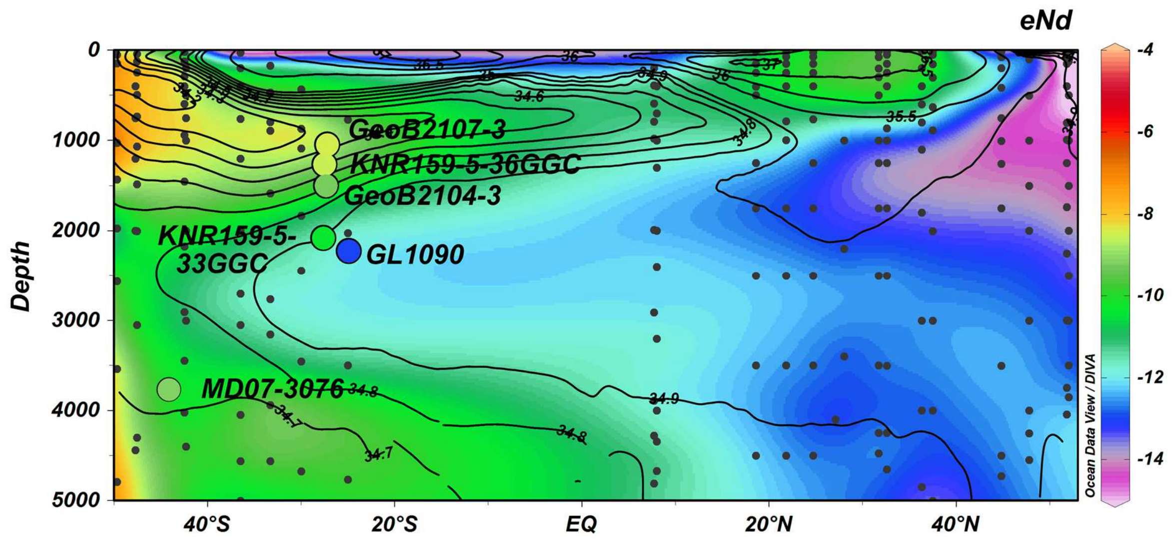

Fig. S3. Interpolated modern seawater ε_{Nd} for the western Atlantic Ocean and eastern Atlantic to south of the Walvis Ridge with the location of seawater measurements given by black dots (Garcia-Solsona et al., 2014; Huang et al., 2014; Jeandel, 1993; Lambelet et al., 2016; Piepgras and Wasserburg, 1987; Stichel et al., 2012). Superimposed are salinity contours (psu; black lines) for the western Atlantic (Antonov et al., 2010). Coloured dots show core top foraminiferal ε_{Nd} values for the South Atlantic cores discussed in this study (colour coded using the same scale as the seawater ε_{Nd}). This figure was produced using the Ocean Data View software (Schlitzer, 2016).

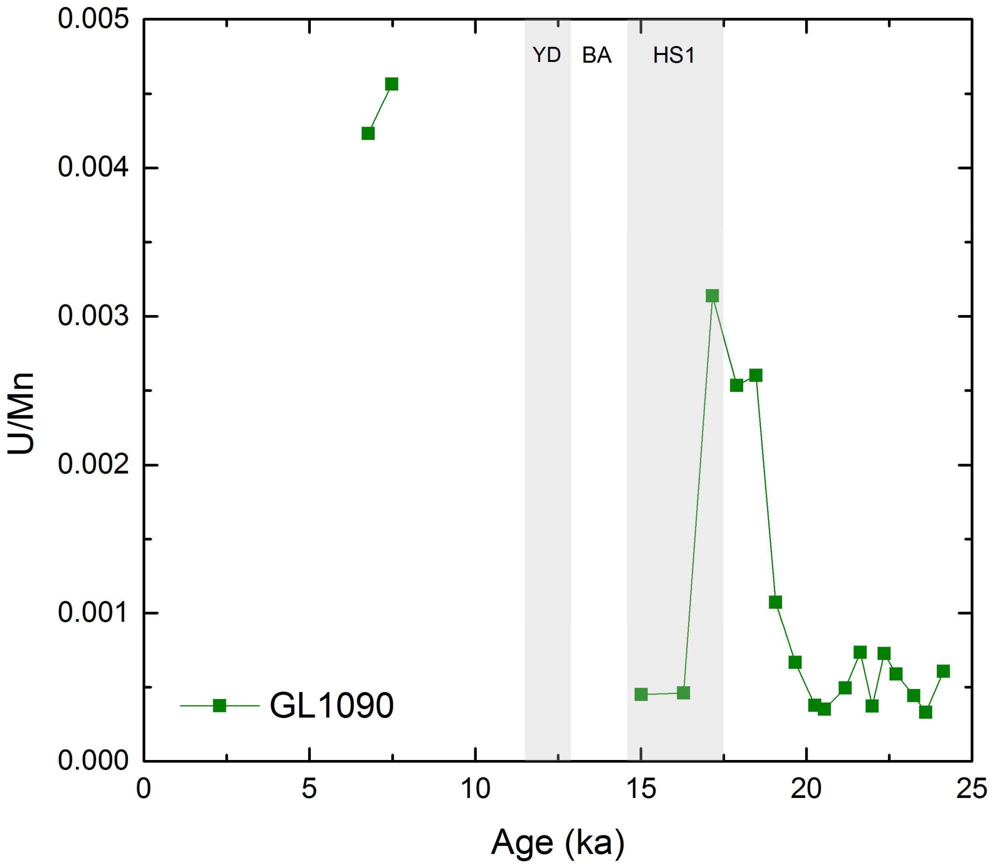

Fig. S4. U/Mn measured on uncleaned foraminifera from core GL1090.

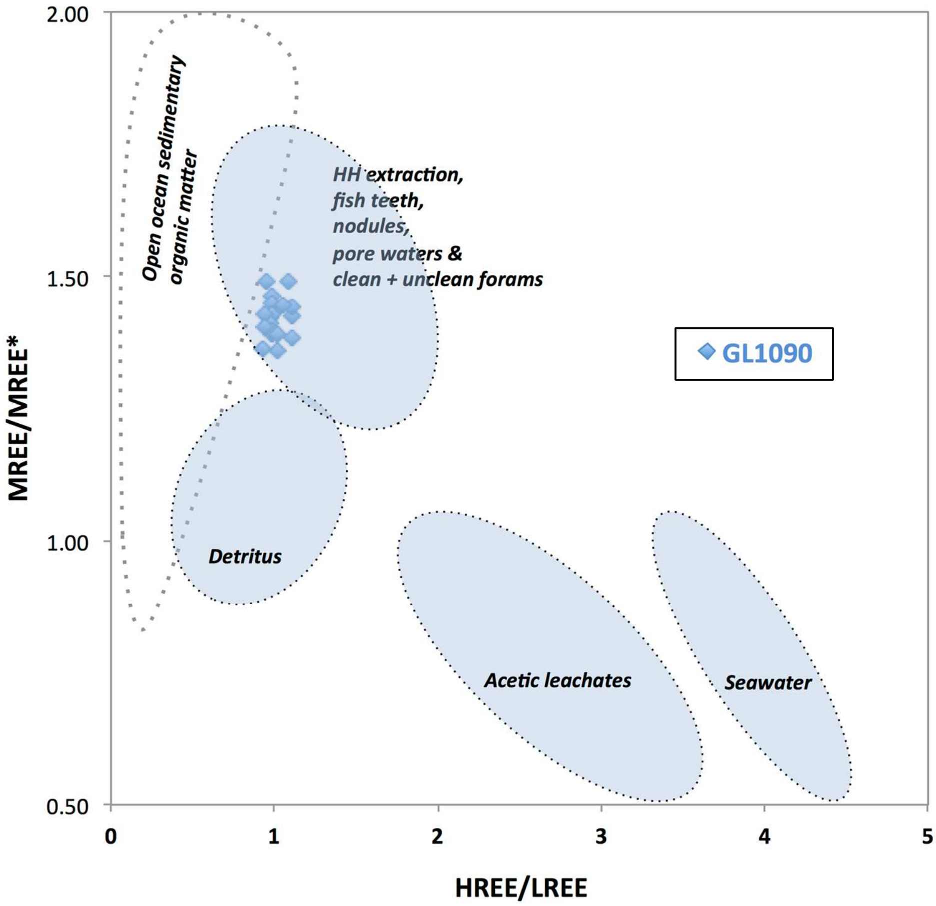

Fig. S5. PAAS-normalized HREE/LREE vs. MREE/MREE* measured on unclean foraminifera samples from core GL1090 in this study. Shaded areas from Martin et al (2010, and references therein) and Molina-Kescher et al (2014, and references therein).

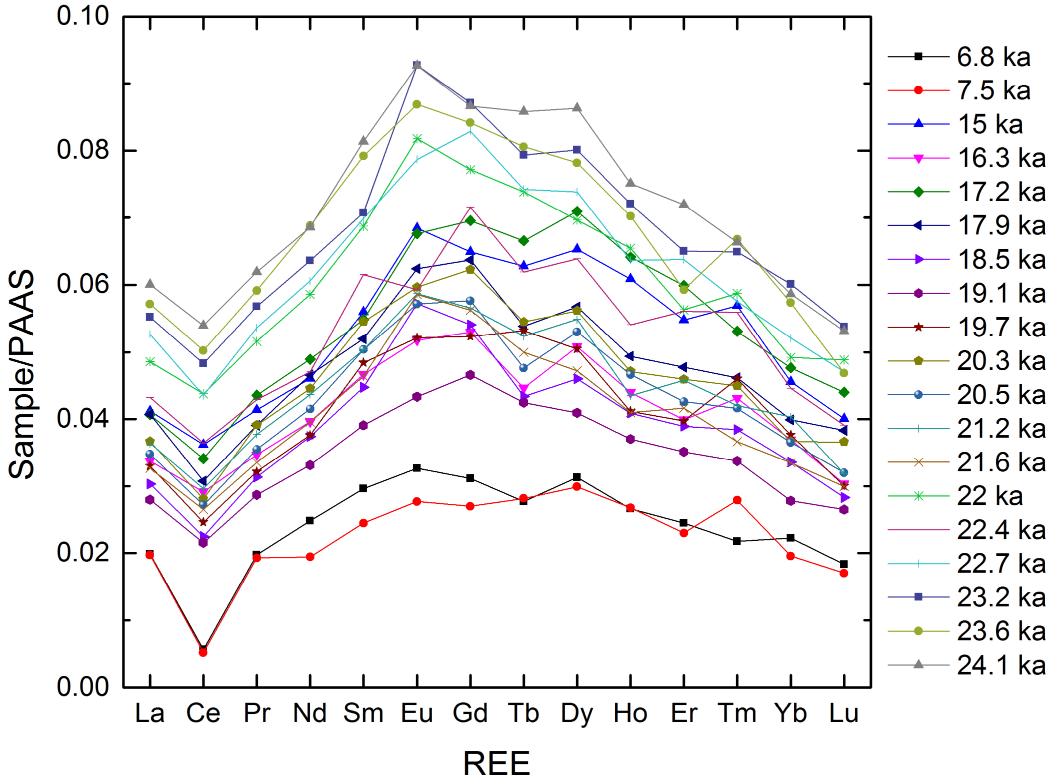

Fig. S6. Rare earth element profiles measured on uncleaned foraminifera from core GL1090. Different time-slices (ka) are given by different colours and symbols as shown in the right-hand column.

Table S1. Cores for which ε_{Nd} and $\delta^{13}C$ records are presented along with data references.

Core	Lat. (°N)	Long. (°E)	Depth (m)	ε_{Nd} reference	$\delta^{13}C$ reference	Age model reference
<u>**South Atlantic**</u>						
GeoB2107-3	-27.2	-46.5	1050	(Howe et al., 2016a)	-	(Heil, 2006)
KNR159-5-36GGC	-27.5	-46.5	1268	(Howe et al., 2016a)	(Curry and Oppo, 2005)	(Lund et al., 2015; Sortor and Lund, 2011)
GeoB2104-3	-27.3	-46.4	1500	(Howe et al., 2016a)	-	(Hickey, 2010)
KNR159-5-33GGC	-27.6	-46.2	2082	*This work*	(Tessin and Lund, 2013)	(Tessin and Lund, 2013)
GL1090	-24.9	-42.5	2225	*This work*	(Santos et al., 2017)	(Santos et al., 2017) *and this work*
MD07-3076	-44.1	-14.2	3770	(Skinner et al., 2013)	(Waelbroeck et al., 2011)	(Skinner et al., 2010)
<u>**North Atlantic**</u>						
SU90-03	40.3	-32.0	2480	(Howe et al., 2016b)	(Chapman and Shackleton, 1998)	(Chapman and Shackleton, 1998) *and this work*

Table S2. Foraminiferal ε_{Nd} of KNR159-5-33GGC

Depth (cm)	**Age (ka)**	**Foraminiferal ε_{Nd}**	**Error (2σ)**
8.5	3.5	-10.3	0.4
16.5	6.4	-10.7	0.5
24.5	9.0	-10.4	0.5
32.5	11.1	-9.9	0.5
40.5	12.8	-9.8	0.5
48.5	14.2	-9.2	0.5
56.5	15.3	-9.3	0.5
64.5	16.1	-9.2	0.5
73.5	16.8	-8.9	0.5
80.5	17.2	-9.4	0.5
96.5	17.7	-9.4	0.5
112.5	18.1	-9.7	0.5
120.5	18.3	-9.5	0.5
128.5	18.5	-9.3	0.5
136.5	18.9	-9.6	0.5
144.5	19.4	-9.0	0.5
152.5	20.2	-9.8	0.5
160.5	21.1	-9.3	0.5
168.5	22.3	-9.2	0.5

Table S3. Detrital ε_{Nd} of KNR159-5-33GGC

Depth (cm)	**Age (ka)**	**Detrital ε_{Nd}**	**Error (2σ)**
8	3.5	-10.9	0.3
15	5.9	-10.6	0.3
23	8.5	-10.8	0.3
33	11.2	-10.1	0.3
39	12.5	-10.3	0.3
47	13.9	-10.0	0.3
55	15.1	-10.3	0.3
63	15.9	-10.3	0.3
73	16.8	-10.4	0.3
79	17.1	-10.4	0.3
95	17.7	-10.4	0.3
113	18.1	-10.4	0.3
119	18.2	-10.5	0.3
127	18.5	-10.4	0.3
136	18.9	-10.4	0.3
143	19.4	-10.5	0.3
152	20.2	-10.4	0.3
160	21.1	-10.4	0.3

Table S4. ε_{Nd} of GL1090

Depth (cm)	Age (ka)	Foraminiferal εNd	Error 2σ	Detrital εNd	Error 2σ	Al/Ca (μmol/mol)
0	6.8	-13.0	0.1	-13.8	0.3	78.5
8	7.5	-13.5	0.1			52.1
10	8.0	-12.8	0.5			
12	8.5	-13.5	0.3			
14	9.1	-13.9	0.3			
16	9.6	-13.9	0.3	-13.8	0.3	
18	10.4	-13.3	0.3			
20	11.3	-13.3	0.2			
22	12.3	-13.4	0.2			
24	13.4	-13.1	0.2	-13.6	0.3	
26	14.6	-12.8	0.2			
28	15.0	-11.1	0.2			42.3
34	16.3	-11.2	0.1	-11.1	0.3	**112**
38	17.2	-11.1	0.1			49.6
42	17.9	-11.1	0.2			**274**
46	18.5	-11.6	0.2			42.8
50	19.1	-11.3	0.1	-12.0	0.3	39.2
54	19.7	-11.0	0.2			16.7
58	20.3	-10.9	0.1			64.6
60	20.5	-10.9	0.1			8.31
66	21.2	-10.9	0.2	-11.4	0.3	17.0
71	21.6	-11.0	0.2			10.4
75	22.0	-10.1	0.2			54.4
79	22.4	-10.3	0.1			6.90
83	22.7	-10.5	0.2			36.6
89	23.2	-10.4	0.1			87.3
93	23.6	-10.4	0.2			**297**
99	24.1	-10.3	0.1			9.63

1085 **Table S5.** Data used in Heinrich Stadial 1 ε_{Nd} section (F=Foraminifera, L=Leachate, FD=Fish
1086 debris, C=Coral)

Name	Lat. (°N)	Long. (°E)	Depth (m)	ε_{Nd}	2σ	Reference	Authigenic phase
KNR159-5-33GGC	-27.6	-46.2	2082	-9.3	0.5	*This work*	F
GL1090	-24.9	-42.5	2225	-11.1	0.1	*This work*	F
ODP 925E	4.2	-43.5	3041	-10.0	0.2	(Howe et al., 2016b)	F
ODP 929B	6.0	-43.7	4356	-9.8	0.4	(Howe et al., 2016b)	F
SU90-03	40.3	-32.0	2475	-11.8	0.3	(Howe et al., 2016b)	F
GeoB2104-3	-27.3	-46.4	1503	-9.4	0.2	(Howe et al., 2016a)	F
KNR159-5-36GGC	-27.5	-46.5	1268	-9.2	0.9	(Howe et al., 2016a)	F
GeoB2107-3	-27.2	-46.5	1048	-8.9	0.1	(Howe et al., 2016a)	F
KNR197-3-46CDH	7.8	-53.7	947	-11.6	1.4	(Huang et al., 2014)	F
KNR197-3-9GGC	7.9	-53.6	1100	-11.4	0.4	(Huang et al., 2014)	F
KNR197-3-25GGC	7.7	-53.8	671	-11.9	0.6	(Huang et al., 2014)	F
GeoB3808-6	-30.8	-14.7	3213	-8.5	0.2	(Jonkers et al., 2015)	L
M35003-4	12.1	-61.2	1299	-9.9	0.2	(Lippold et al., 2016)	L
U1313	41.0	-33.0	3426	-13.7	0.4	(Lang et al., 2016; Lippold et al., 2016)	L, FD
12JPC	29.7	-72.9	4250	-10.1	1.1	(Lippold et al., 2016)	L
GeoB1515-1	4.2	-43.7	3129	-10.1	0.1	(Lippold et al., 2016)	L
GeoB1523-1	3.8	-41.6	3292	-10.1	0.6	(Lippold et al., 2016)	L
ODP 1089	-40.9	9.9	4621	-7.1	0.5	(Lippold et al., 2016)	L
RC11-83	-41.1	9.7	4718	-7.1	1.1	(Piotrowski et al., 2004)	L
OCE326-GGC6	33.7	-57.6	4540	-10.9	0.6	(Roberts et al., 2010)	F

Coral 47396	-59.4	-68.5	1125	-6.4	0.3	(Robinson and van de Flierdt, 2009)	C
MD07 3076	-44.1	-14.2	3770	-6.3	0.6	(Skinner et al., 2013)	F
MD02-2594	-34.7	17.3	2440	-8.2	0.3	(Wei et al., 2016)	L
GeoB3603-2	-35.1	17.6	2840	-7.6	0.1	(Wei et al., 2016)	L
ALV-3890-1742-007-001	38.2	-60.5	1381	-11.3	0.2	(Wilson et al., 2014)	C
1700-1800 m average	38.1	-60.2	1766	-12.0	1.0	(Wilson et al., 2014)	C
ALV-3890-1330-002-007	38.2	-60.5	1886	-13.3	0.2	(Wilson et al., 2014)	C
2000-2100 m average	33.8	-62.6	2070	-13.7	1.4	(Wilson et al., 2014)	C
2200-2300 m average	33.8	-62.6	2247	-12.3	1.7	(Wilson et al., 2014)	C
ALV-3887-1549-004-various	33.8	-62.6	2372	-12.0	1.8	(Wilson et al., 2014)	C
ALV-3887-1436-003-003	33.8	-62.6	2441	-14.1	0.2	(Wilson et al., 2014)	C

Table S6. Data used to construct the Last Glacial Maximum ε_{Nd} section (F = Foraminifera, L=Leachate, HRC =High-resolution crust, FD=Fish debris)

Name	Lat. (°N)	Long. (°E)	Depth (m)	ε_{Nd}	2σ	Reference	Authigenic phase
KNR159-5-33GGC	-27.6	-46.2	2082	-9.5	0.5	*This work*	F
CH115 70	-30.0	-36.0	2340	-8.6	0.1	(Howe et al., 2016)	F
GeoB2104-3	-27.3	-46.4	1503	-9.2	0.2	(Howe et al., 2016)	F
GeoB2107-3	-27.2	-46.5	1048	-8.8	0.1	(Howe et al., 2016)	F
GL1090	-24.9	-42.5	2225	-10.9	0.1	(Howe et al., 2016)	F
MD96 2085	-30.0	13.0	3001	-8.6	0.3	(Howe et al., 2016)	F
MD96 2086	-29.8	12.1	3606	-7.8	0.2	(Howe et al., 2016)	F
MD96 2098	-25.6	12.6	2910	-9.3	0.2	(Howe et al., 2016)	F
ODP 668A	4.8	-20.9	2693	-11.6	0.1	(Howe et al., 2016)	F
ODP 925E	4.2	-43.5	3041	-9.8	0.3	(Howe et al., 2016)	F
ODP 928B	5.5	-43.7	4011	-9.5	0.3	(Howe et al., 2016)	F
ODP 929B	6.0	-43.7	4356	-9.2	0.2	(Howe et al., 2016)	F
ODP 1088	-41.0	13.5	2082	-7.7	0.3	(Howe et al., 2016)	F
RC 11 86	-36.0	18.0	2829	-8.0	0.1	(Howe et al., 2016)	F
RC 12 267	-39.0	-26.0	4144	-4.9	0.2	(Howe et al., 2016)	F
RC 12 294	-37.0	-10.0	3308	-7.0	0.3	(Howe et al., 2016)	F
RC 13 228	-22.0	11.0	3204	-8.9	0.6	(Howe et al., 2016)	F
RC 13 229	-26.0	11.0	4194	-7.7	0.2	(Howe et al., 2016)	F
RC 13 253	-46.0	7.0	2494	-8.3	0.3	(Howe et al., 2016)	F
RC 15 94	-43.0	-21.0	3762	-5.0	1.2	(Howe et al., 2016)	F
SU90-03	40.3	-32.0	2475	-10.9	0.1	(Howe et al., 2016)	F
TTN057-6 PC4	-42.9	8.6	3702	-6.4	0.1	(Howe et al., 2016)	F
V 22 174	-10.0	-12.0	2630	-10.1	0.2	(Howe et al., 2016)	F
V 25 42	12.0	-51.0	4707	-9.6	0.4	(Howe et al., 2016)	F
V 25 59	1.4	-33.5	3824	-9.8	0.2	(Howe et al., 2016)	F
KNR159-5-36GGC	-27.5	-46.5	1268	-8.9	0.5	(Howe et al., 2016a)	F
TR079 D-14	16.9	-61.2	2000	-12.1	0.7	(Foster et al., 2007)	HRC
BM1969.05	39.0	-61.0	1800	-12.6	0.6	(Foster et al., 2007)	HRC
KNR140-31GGC	30.9	-74.5	3410	-10.3	0.3	(Gutjahr et al., 2008)	L
KNR140-12JPC	29.1	-72.9	4250	-10.3	0.7	(Gutjahr et al., 2008)	L
KNR197-3-25GGC	7.7	-53.8	671	-10.3	0.3	(Huang et al., 2014)	F
KNR197-3-46CDH	7.8	-53.7	947	-10.5	0.3	(Huang et al., 2014)	F
KNR197-3-9GGC	7.9	-53.6	1100	-10.9	0.3	(Huang et al., 2014)	F
GeoB3808-6	-30.8	-14.7	3213	-7.5	0.3	(Jonkers et al., 2015)	L
M35003-4	12.1	-61.2	1299	-10.3	0.9	(Lippold et al., 2016)	L

U1313	41.0	-33.0	3426	-11.6	1.0	(Lang et al., 2016; Lippold et al., 2016)	L, FD
GeoB1515-1	4.2	-43.7	3129	-9.9	0.4	(Lippold et al., 2016)	L
GeoB1523-1	3.8	-41.6	3292	-10.4	0.5	(Lippold et al., 2016)	L
ODP 1089	-40.9	9.9	4621	-7.5	0.9	(Lippold et al., 2016)	L
TNO57-21	-41.1	7.9	4981	-6.8	0.5	(Piotrowski et al., 2012)	F
OCE326-GGC6	33.7	-57.6	4540	-10.4	0.5	(Roberts et al., 2010)	F
MD07 3076	-44.1	-14.2	3770	-5.7	0.4	(Skinner et al., 2013)	F
MD02-2594	-34.7	17.3	2440	-7.8	0.4	(Wei et al., 2016)	F
GeoB3603-2	-35.1	17.6	2840	-8.0	0.3	(Wei et al., 2016)	FD

Table S7. Difference between Heinrich Stadial 1 and Last Glacial Maximum ε_{Nd} data. Please see Tables S5 and S6 for the references of the previously published data.

Name	Lat. (°N)	Long. (°E)	Depth (m)	HS1 - LGM ε_{Nd}	Combined 2σ
KNR159-5-33GGC	-27.6	-46.2	2082	*0.3*	*1.2*
GeoB2104-	-27.3	-46.4	1503	*-0.1*	*0.3*
GeoB2107-3	-27.2	-46.5	1048	*-0.1*	*0.3*
GL1090	-24.9	-42.5	2225	*-0.2*	*0.3*
ODP 925E	4.2	-43.5	3041	*-0.2*	*0.5*
ODP 929B	6.0	-43.7	4356	*-0.6*	*1.1*
SU90-03	40.3	-32.0	2475	*-0.9*	*0.4*
KNR159-5-36GGC	-27.5	-46.5	1268	*-0.5*	*2.1*
KNR140-12JPC	29.1	-72.9	4250	*0.2*	*1.8*
KNR197-3-25GGC	7.7	-53.8	671	*-1.6*	*0.9*
KNR197-3-46CDH	7.8	-53.7	947	*-1.1*	*1.7*
KNR197-3-9GGC	7.9	-53.6	1100	*-0.4*	*0.7*
M35003-4	12.1	-61.2	1299	*0.3*	*1.1*
U1313	41.0	-33.0	3426	*-2.1*	*1.4*
GeoB1515-1	4.2	-43.7	3129	*-0.2*	*0.5*
GeoB1523-1	3.8	-41.6	3292	*0.2*	*1.1*
ODP 1089	-40.9	9.9	4621	*0.4*	*1.4*
GeoB3808-6	-30.8	-14.7	3213	*-1.0*	*0.5*
OCE326-GGC6	33.7	-57.6	4540	*-0.5*	*1.1*
MD07 3076	-44.1	-14.2	3770	*-0.6*	*1.0*
MD02-2594	-34.7	17.3	2440	*-0.4*	*0.7*

GeoB3603-2	-35.1	17.6	2840	*0.4*	*0.4*

References

Antonov, J.I., Seidov, D., Boyer, T.P., Locarnini, R.A., Mishonov, A. V., Garcia, H.E., Baranova, O.K., Zweng, M.M., Johnson, D.R., 2010. World Ocean Atlas 2009, Volume 2: Salinity. U.S. Government Printing Office.

Chapman, M.R., Shackleton, N.J., 1998. Millennial-scale fluctuations in North Atlantic heat flux during the last 150,000 years. Earth Planet. Sci. Lett. 159, 57–70.

Chapman, M.R., Shackleton, N.J., Duplessy, J.-C., 2000. Sea surface temperature variability during the last glacial-interglacial cycle: assessing the magnitude and pattern of climate change in the North Atlantic. Palaeogeogr. Palaeoclimatol. Palaeoecol. 157, 1–25.

Curry, W.B., Oppo, D.W., 2005. Glacial water mass geometry and the distribution of $\delta^{13}C$ of ΣCO_2 in the western Atlantic Ocean. Paleoceanography 20, PA1017. doi:10.1029/2004PA001021

Foster, G.L., Vance, D., Prytulak, J., 2007. No change in the neodymium isotope composition of deep water exported from the North Atlantic on glacial-interglacial time scales. Geology 35, 37–40. doi:10.1130/G23204A.1

Garcia-Solsona, E., Jeandel, C., Labatut, M., Lacan, F., Vance, D., Chavagnac, V., Pradoux, C., 2014. Rare earth elements and Nd isotopes tracing water mass mixing and particle-seawater interactions in the SE Atlantic. Geochim. Cosmochim. Acta 125, 351–372. doi:10.1016/j.gca.2013.10.009

Gutjahr, M., Frank, M., Stirling, C.H., Keigwin, L.D., Halliday, A.N., 2008. Tracing the Nd isotope evolution of North Atlantic Deep and Intermediate Waters in the western North Atlantic since the Last Glacial Maximum from Blake Ridge sediments. Earth Planet. Sci. Lett. 266, 61–77. doi:10.1016/j.epsl.2007.10.037

Heil, G., 2006. Abrupt climate shifts in the western tropical to subtropical Atlantic region during the last glacial. Bremen University

Howe, J.N.W., Piotrowski, A.M., Noble, T.L., Mulitza, S., Chiessi, C.M., Bayon, G., 2016. North Atlantic Deep Water production during the Last Glacial Maximum. Nat. Commun. 7, 1–8. doi:10.1038/ncomms11765

Howe, J.N.W., Piotrowski, A.M., Oppo, D.W., Huang, K., Mulitza, S., Chiessi, C.M., Blusztajn, J., 2016a. Antarctic intermediate water circulation in the South Atlantic over the past 25,000 years. Paleoceanography 1–13. doi:10.1002/2016PA002975.

Howe, J.N.W., Piotrowski, A.M., Rennie, V.C.F., 2016b. Abyssal origin for the early Holocene pulse of unradiogenic neodymium isotopes in Atlantic seawater. Geology 831, 831–834. doi:10.1130/G38155.1

Huang, K.-F., Oppo, D.W., Curry, W.B., 2014. Decreased influence of Antarctic intermediate water in the tropical Atlantic during North Atlantic cold events. Earth Planet. Sci. Lett. 389, 200–208. doi:10.1016/j.epsl.2013.12.037

Jeandel, C., 1993. Concentration and isotopic composition of Nd in the South Atlantic Ocean. Earth Planet. Sci. Lett. 117, 581–591.

Jonkers, L., Zahn, R., Thomas, A., Henderson, G., Abouchami, W., François, R., Masque, P., Hall, I.R., Bickert, T., 2015. Deep circulation changes in the central South Atlantic during the past 145 kyrs reflected in a combined $^{231}Pa/^{230}Th$, Neodymium isotope and benthic $\delta^{13}C$ records. Earth Planet. Sci. Lett. 419, 14–21. doi:10.1016/j.epsl.2015.03.004

Lambelet, M., van de Flierdt, T., Crocket, K., Rehkämper, M., Kreissig, K., Coles, B., Rijkenberg, M.J.A., Gerringa, L.J.A., de Baar, H.J.W., Steinfeldt, R., 2016. Neodymium isotopic composition and concentration in the western North Atlantic Ocean: results from the GEOTRACES GA02 section. Geochim. Cosmochim. Acta 177, 1–29. doi:10.1016/j.gca.2015.12.019

Lang, D.C., Bailey, I., Wilson, P.A., Chalk, T.B., Foster, G.L., Gutjahr, M., 2016. Incursions of southern-sourced water into the deep North Atlantic during late Pliocene glacial intensification. Nat. Geosci. 9, 375–379. doi:10.1038/ngeo2688

Lippold, J., Gutjahr, M., Blaser, P., Christner, E., Ferreira, M.L.D.C., Mulitza, S., Christl, M., Wombacher, F., Böhm, E., Antz, B., Cartapanis, O., Vogel, H., Jaccard, S.L., 2016. Deep water provenience and dynamics of the (de)glacial Atlantic meridional overturning circulation. Earth Planet. Sci. Lett. 445, 68–78. doi:10.1016/j.epsl.2016.04.013

Lund, D.C., Tessin, A.C., Hoffman, J.L., Schmittner, A., 2015. Southwest Atlantic water mass evolution during the last deglaciation. Paleoceanography 30. doi:10.1002/2014PA002657.

Martin, E. E., Blair, S. W., Kamenov, G. D., Scher, H. D., Bourbon, E., Basak, C., Newkirk, D. N., 2010. Extraction of Nd isotopes from bulk deep sea sediments for paleoceanographic studies on Cenozoic time scales. Chem. Geol. 269, 414-431.

McManus, J.F., Francois, R., Gherardi, J.-M., Keigwin, L.D., Brown-Leger, S., 2004. Collapse and rapid resumption of Atlantic meridional circulation linked to deglacial climate changes. Nature 428, 834–837. doi:10.1038/nature02494

Molina-Kescher, M., Frank, M., Hathorne, E. C., 2014. Nd and Sr isotope compositions of different phases of surface sediments in the South Pacific: Extraction of seawater signature, boundary exchnage, and detrital/dust provenance. Geochem. Geophys. Geosyst. 15, 3502-3520.

Parnell, A.C., Haslett, J., Allen, J.R.M., Buck, C.E., Huntley, B., 2008. A flexible approach to assessing synchroneity of past events using Bayesian reconstructions of sedimentation history. Quat. Sci. Rev. 27, 1872–1885.

Piepgras, D.J., Wasserburg, G.J., 1987. Rare earth element transport in the western North Atlantic inferred from Nd isotopic observations. Geochim. Cosmochim. Acta 51, 1257–1271. doi:10.1016/0016-7037(87)90217-1

Piotrowski, A.M., Galy, A., Nicholl, J.A.L., Roberts, N., Wilson, D.J., Clegg, J.A., Yu, J., 2012. Reconstructing deglacial North and South Atlantic deep water sourcing using foraminiferal Nd isotopes. Earth Planet. Sci. Lett. 357-358, 289–297.

Reimer, P., Bard, E., Bayliss, A., Beck, J.W., Blackwell, P.G., Ramsey, C.B., Buck, C.E., Cheng, H., Edwards, R.L., Friedrich, M., Grootes, P.M., Guilderson, T.P., Haflidason, H., Hajdas, I., Hatté, C., Heaton, T.J., Hoffman, D.L., Hogg, A.G., Hughen, K.A., Kaise, K.F., Kromer, B., Manning, S.W., Niu, M., Reimer, R.W., Richard, D.A., Scott, E.M., Southon, J.R., Staff, R.A., Turney, C.S.M., Plicht, J. van der, 2013. IntCal13 and Marine13 Radiocarbon Age Calibration Curves 0–50,000 Years cal BP. Radiocarbon 55, 1869–1887. doi:10.2458/azu_js_rc.55.16947

Roberts, N.L., Piotrowski, A.M., McManus, J.F., Keigwin, L.D., 2010. Synchronous deglacial overturning and water mass source changes. Science 327, 75–78. doi:10.1126/science.1178068

Robinson, L.F., van de Flierdt, T., 2009. Southern Ocean evidence for reduced export of North Atlantic Deep Water during Heinrich event 1. Geology 37, 195–198. doi:10.1130/G25363A.1

Santos, T.P., Lessa, D.O., Venancio, I.M., Chiessi, C.M., Mulitza, S., Kuhnert, H., Govin, A., Machado, T., Costa, K.B., Toledo, F., Dias, B.B., Albuquerque, A.L.S., 2017. Prolonged warming of the Brazil Current precedes deglaciations. Earth Planet. Sci. Lett. 463, 1-12.

Schlitzer, R., 2016. Ocean Data View [WWW Document]. URL http://odv.awi.de

Skinner, L.C., Fallon, S., Waelbroeck, C., Michel, E., Barker, S., 2010. Ventilation of the deep Southern Ocean and deglacial CO2 rise. Science 328, 1147–1151. doi:10.1126/science.1183627

Skinner, L.C., Scrivner, A.E., Vance, D., Barker, S., Fallon, S., Waelbroeck, C., 2013. North Atlantic versus Southern Ocean contributions to a deglacial surge in deep ocean ventilation. Geology 41, 667–670. doi:10.1130/G34133.1

Sortor, R.N., Lund, D.C., 2011. No evidence for a deglacial intermediate water $\Delta^{14}C$ anomaly in the SW Atlantic. Earth Planet. Sci. Lett. 310, 65–72. doi:10.1016/j.epsl.2011.07.017

Stichel, T., Frank, M., Rickli, J., Haley, B.A., 2012. The hafnium and neodymium isotope composition of seawater in the Atlantic sector of the Southern Ocean. Earth Planet. Sci. Lett. 317-318, 282–294. doi:10.1016/j.epsl.2011.11.025

Taylor, S.R., McLennan, S., 1985. The Continental Crust: Its composition and evolution. Blackwell Scientific, Oxford. 312 pp.

Tessin, A.C., Lund, D.C., 2013. Isotopically depleted carbon in the mid-depth South Atlantic during the last deglaciation. Paleoceanography 28, 296–306. doi:10.1002/palo.20026

Waelbroeck, C., Skinner, L.C., Labeyrie, L., Duplessy, J.-C., Michel, E., Vazquez Riveiros, N., Gherardi, J.-M., Dewilde, F., 2011. The timing of deglacial circulation changes in the Atlantic. Paleoceanography 26, PA3213. doi:10.1029/2010PA002007

Wei, R., Abouchami, W., Zahn, R., Masque, P., 2016. Deep circulation changes in the South Atlantic since the Last Glacial Maximum from Nd isotope and multi-proxy records. Earth Planet. Sci. Lett. 434, 18–29. doi:10.1016/j.epsl.2015.11.001

Wilson, D.J., Crocket, K.C., van de Flierdt, T., Robinson, L.F., Adkins, J.F., 2014. Dynamic intermediate ocean circulation in the North Atlantic during Heinrich Stadial 1: a radiocarbon and neodymium isotope perspective. Paleoceanography 29, 1072–1093. doi:10.1002/2014PA002674